Geochemistry, Geophysics, Geosystems

RESEARCH ARTICLE
10.1029/2019GC008262

Observation and Simulation of Solid Sedimentary Flux: Examples From Northwest Africa

Bhavik Harish Lodhia[1], Gareth G. Roberts[1], Alastair J. Fraser[1], Jerry Jarvis[2], Richard Newton[2], and Robbie J. Cowan[2]

[1]Department of Earth Science and Engineering, Imperial College London, London, UK, [2]Tullow Oil Plc., London, UK

Abstract The sedimentary archive preserved at passive margins provides important clues about the evolution of continental topography. For example, histories of African uplift, erosion, and deposition of clastic sedimentary rock provide information about mantle convection. Furthermore, relating histories of uplift and erosion from regions where sediment is generated to measurements of efflux is important for understanding basin evolution and the distribution of natural resources. We focus on constraining Mesozoic to Recent solid sedimentary flux to northwest Africa's passive margin, which today is fed by rivers draining dynamically supported topography. Histories of sedimentary flux are calculated by mapping stratigraphy using seismic reflection and well data courtesy of Tullow Oil Plc and TGS. Stratigraphic ages, conversion from two-way time to depth and compaction, are parameterized using biostratigraphic and check-shot records from exploration, International Ocean Discovery Program and Deep Sea Drilling Project wells. Results indicate that Late Cretaceous to Oligocene (~100–23 Ma) sedimentary flux decreased gradually. A slight increase in Neogene sedimentary flux is observed, which is concomitant with a change from carbonate to clastic sedimentation. Pliocene to Recent (~5–0 Ma) flux increased by an order of magnitude. This history of sedimentary flux and facies change is similar to histories observed at other African deltas. To constrain sources of sedimentary flux, 14,700 longitudinal river profiles were inverted to calculate a history of continental uplift. These results were used to parameterize a simple "source-to-sink" model of fluvial erosion and sedimentary efflux. Results suggest that increased clastic flux to Africa's deltas from ~30 Ma was driven by denudation induced by dynamic support.

Key Points:
- Mesozoic to Recent solid sedimentary flux from West African seismic and well data
- Predict sedimentary flux histories from inversion of 14,700 African river profiles
- Neogene uplift of dynamically supported swells generated punctuated sedimentary flux

Supporting Information:
- Supporting Information S1

Correspondence to:
B. H. Lodhia and G. G. Roberts,
b.lodhia14@imperial.ac.uk;
gareth.roberts@imperial.ac.uk

Citation:
Lodhia, B. H., Roberts, G. G., Fraser, A. J., Jarvis, J., Newton, R., & Cowan, R. J. (2019). Observation and simulation of solid sedimentary flux: Examples from northwest Africa. *Geochemistry, Geophysics, Geosystems*, *20*. https://doi.org/10.1029/2019GC008262

Received 11 FEB 2019
Accepted 31 AUG 2019
Accepted article online 1 OCT 2019

©2019. American Geophysical Union. All Rights Reserved.

1. Introduction

Records of clastic efflux to passive margins contain information about histories of tectonic and erosional processes. They provide clues about longevity of topography and erosional processes, and in regions of dynamic support the sedimentary archive can constrain length scale and time scale of mantle convective processes (e.g., Allen, 2008; Clift & Sun, 2006; Czarnota et al., 2014; Lodhia et al., 2018; Rouby et al., 2009; Somme et al., 2011; Walford et al., 2005). Furthermore, constraining sources of sedimentary rock and their history of deposition is critical for understanding the origin and distribution of natural resources including hydrocarbon reservoirs (e.g., Somme et al., 2011; Vear, 2005). Our approach to tackling these problems centers on measuring rates of sedimentary efflux to passive margins recorded by stratigraphy and using continental drainage patterns to predict histories of uplift rate, erosion, and sedimentary flux in source regions. We focus on calculating rates and volumes of Mesozoic to Recent solid sedimentary flux to the Mauritanian margin of West Africa, which is drained by several large rivers that are sourced atop long wavelength, dynamically supported, topographic swells (Figures 1 and 2).

1.1. African Uplift

It is generally accepted that convective flow in the sublithospheric mantle has generated African topography during the last 30 Ma (e.g., Burke, 1996; Moucha & Forte, 2011; Nyblade & Robinson, 1994; Paul et al., 2014; Rudge et al., 2015). Its topography is strongly bimodal. Subequatorial Africa is characterized by a broad superswell with a wavelength of $O(10^4)$ km, while northern Africa is generally low lying (Nyblade & Robinson, 1994). Superimposed on this bimodal framework are smaller domal swells with wavelengths of $O(10^3)$ km (Burke, 1996; Holmes, 1944). Widespread volcanic activity, basin subsidence, uplifted domes (e.g., Bié, Hoggar, Tibesti and Fouta Djallon; Figures 1 and 2), and extension at the East African Rift characterize present-day African topography (e.g., Burke, 1996; Crosby et al., 2010; Moucha & Forte, 2011). Estimates of

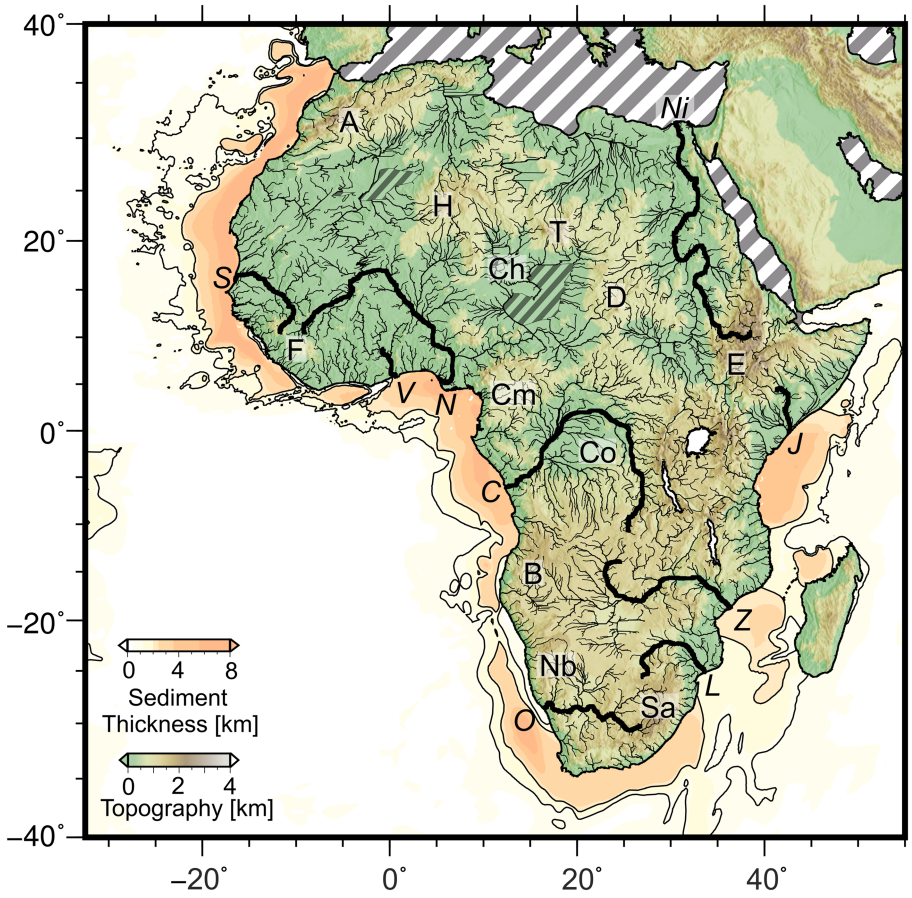


Figure 1. African topography, drainage, and sedimentary rock offshore. Black lines onshore = drainage networks extracted from 90 × 90 m Shuttle Radar Topography Mission data set. Thick black lines = principal African rivers, *S* = Senegal,*V* = Volta, *N* = Niger, *C* = Congo, *O* = Orange, *L* = Limpopo, *Z* = Zambezi, *J* = Jubba-Shebelle and *Ni* = Nile. Topographic swell labels: A = Atlas, F = Fouta-Djallon, H = Hoggar. T = Tibesti, D = Darfur, Cm = Cameroon, B = Bíe, Nb = Namibia, Sa = South Africa, E = Ethiopian Plateau. Continental basins labeled Co = Congo and Ch = Chad. Thin hatching pattern covers region with unreliable drainage extraction. Offshore sediment thickness from Whittaker et al. (2013). Contours indicate thicknesses of 2 and 4 km.

dynamic topography calculated using long wavelength (800–2,500 km) components of the EIGEN6c GOCE gravity field and an admittance $Z = 35 \pm 10$ mGal/km is shown in Figure 2 (Crosby et al., 2010; Förste et al., 2014; Hoggard et al., 2017; McKenzie & Fairhead, 1997). These results imply that the Bié, Namibian, South African, and North African swells (e.g., Atlas, Fouta Djallon, Hoggar, and Tibesti) are dynamically supported by sublithospheric density anomalies. Radial drainage patterns are centered on many of these swells (Figure 2), and many areas of low topography have dendritic drainage networks (e.g., Congo; Figure 2a). If $Z = 45 \pm 10$ mGal/km, which is probably more appropriate for central Africa, calculated subplate support is reduced by a factor of ~0.8 (e.g., Jones et al., 2012). These observations suggest that subplate processes determine the pattern of drainage across the African continent. A subset of these continental drainage patterns have been used to invert for smooth spatiotemporal histories of uplift, which yields results that are consistent with the notion that many of Africa's domal swells grew during the last ~ 30 Ma (Paul et al., 2014; Pritchard et al., 2009; Roberts et al., 2012b; Rudge et al., 2015).

1.2. Northwest Africa

Bringing together observations of continental uplift and erosion with offshore sedimentary deposition is a step toward generating a predictive framework for the African "source-to-sink" sedimentary routing system. We focus on the northwest African margin and the Mauritanian basin, which has probably been relatively tectonically stable following Middle Jurassic separation from Gondwana (e.g., Davison, 2005). The Mauritanian basin forms the northern part of the larger Mauritania-Senegal-Guinea-Bissau-Conarky (MSGBC) Basin. Today, this region is drained by rivers that carry sediment through the Mauritanides fold belt, which

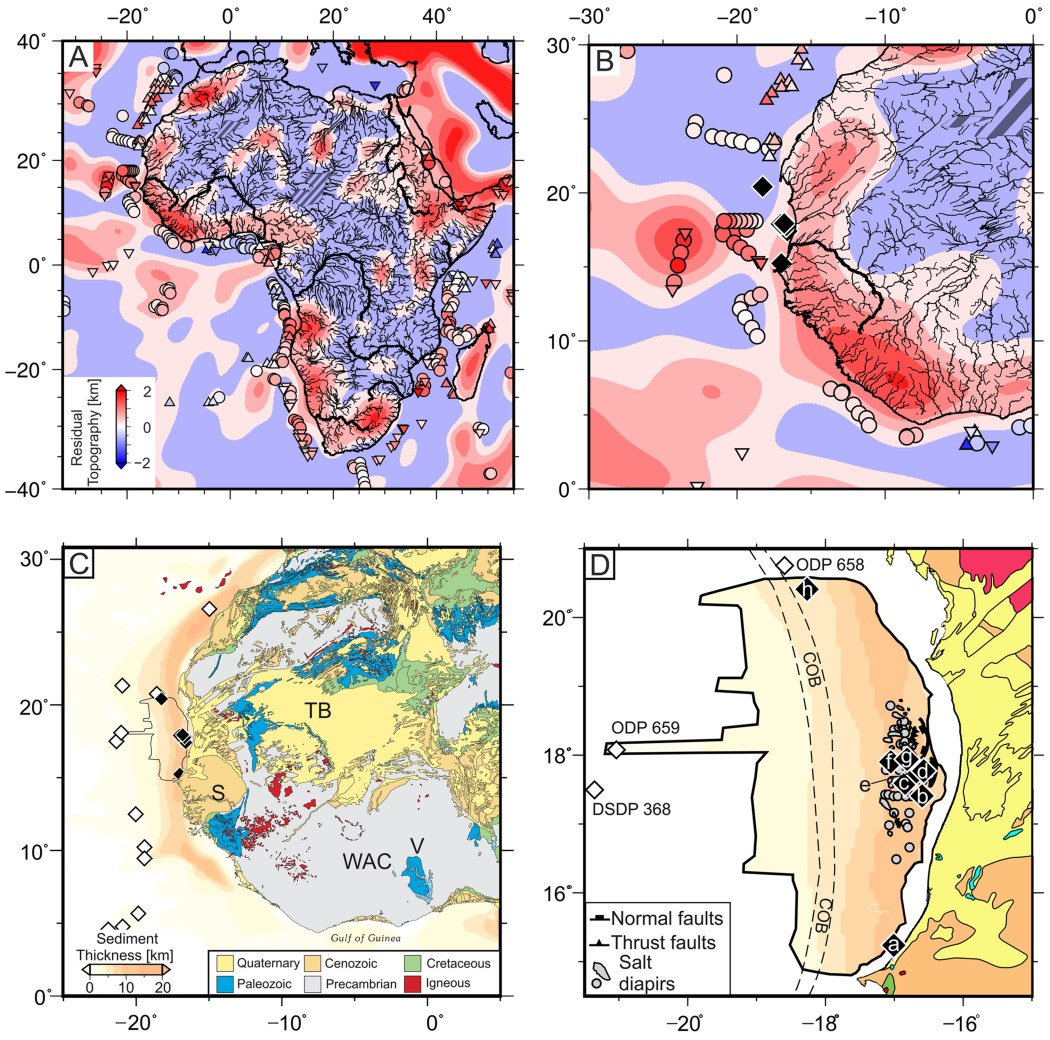


Figure 2. Subplate support and drainage patterns of the Mauritanian margin and its surroundings. (a) Red/white/blue color scale = dynamic topography calculated using long wavelength (~ 800–2,500 km) free air gravity data from GOCE data set and an admittance $Z = 35$ mGal/km, contour interval = 10 mGal ≈ 0.35 km; if $Z = 45 \pm 10$ mGal/km, which is probably appropriate for central Africa, calculated dynamic support is reduced by a factor of 0.8 (see, e.g., Förste et al., 2014; Jones et al., 2012). Thin/thick black curves = drainage networks extracted from Shuttle Radar Topography Mission digital elevation model (see Figure 1). Circles/triangles = accurate/upper or lower bound estimates of residual ocean age-depths (Hoggard et al., 2017; Lodhia et al., 2018). (b) Residual topography in study area. Black diamonds = exploration wells used in this study. Note radial drainage patterns atop Africa's domal swells. (c) Geological map and offshore sedimentary thickness of West Africa (after Brownfield & Charpentier, 2003; Lodhia et al., 2018; Whittaker et al., 2013). S = Senegal; TB = Tauodenni basin; WAC = West African craton; V = Volta. Black/white diamonds = exploration/Ocean Discovery Program (ODP) and Deep Sea Drilling Project (DSDP) wells used in this study. Thin black polygon offshore Mauritania = extent of seismic data. (d) Sediment thickness from Whittaker et al. (2013). Black polygon = region covered by seismic survey used in this study; dashed lines labeled COB = continent-ocean boundary mapped from reflection seismic data.

extends from the northern High Atlas of Morocco to southern Senegal, and disgorge into the Atlantic Ocean (Villeneuve, 2005; Figure 2). The modern Senegal catchment drains the northern part of the Fouta Djallon swell and delivers sediment to the Atlantic Ocean at rates of ~3 Mt/year (Milliman & Farnsworth, 2013). Atop the Fouta Djallon swell drainage networks are arranged in a broadly radial pattern. Rivers draining into the Atlantic margin of northwest Africa are bounded to the north by the Atlas mountains. This topographic swell is also drained by fluvial networks with an approximately radial pattern (Figure 2). The elevation and dip of shallow marine and lacustrine Miocene sedimentary rock indicate that the Atlas Mountains experienced ~1 km of long wavelength postorogenic uplift, which has been attributed to subplate support (Babault et al., 2008). Offshore, seismic tomography and backstripped stratigraphy indicate that mantle convective

Table 1
Summary of Wells Used in This Study

Well	Water depth (m)	First sample depth (km)	Total depth (m)	Stratigraphic range	Benthonic biofacies (e.g.)	Paleo-water depth
A	79	~0.3	3,167	Eocene-Albian	*Triorites africaensis and Cibicides lobatulus*	
B	172	~1.3	4,977	Pliocene-Upper Jurassic	*Gabonisporis vigourpxi & Lucianorhabdus compactus*	UB-N
C	1,266	~2.2	3,080	Miocene	*Bulmina costata*	MB
D	281	~1.0	2,608	Miocene-Eocene	*Cibicidoides grosseperforatus*	UB-LB
E	490	~1.4	2,715	Miocene-Eocene	*Epinoides vicksburgenis*	UB
F	1,776	~2.7	3,060	Miocene-Eocene	*Bulimina costata & Turborotalia passagnoensis*	UB-LB
G	1,120	~2.1	2,908	Miocene-Oligocene	*Bulmina striata & Caenopedina cubensis*	MB-LB
H	1,414	~1.9	3,299	Eocene-Upper Cretaceous	*Cibicidoides grimsdale*	B

Note. Paleo-water depths are based on the following definitions from Immenhauser (2009): Neritic (N) = 0–150 m; upper bathyal (UB) = 150–500 m, middle bathyal (MB) = 500–2,000 m; lower bathyal (LB) = >2,000 m; bathyal (B) = >150 m.

drawdown of the Mauritanian basin has led to 0.4–0.8 km of Miocene-Recent water-loaded subsidence (Lodhia et al., 2018).

Hydrocarbon exploration offshore northwest Africa has generated a body of seismic and well data that constrain the stratigraphy of the margin. Gas discoveries have been made in Upper Cretaceous sandstone reservoirs in the Pelican, Tortue, and Yakaar fields in the MSGBC Basin. Oil discoveries at the Chinguetti and Tiof fields have been made in Cenozoic sandstone reservoirs and are probably charged by Cenomanian-Turonian source rocks (Brownfield & Charpentier, 2003; Davison, 2005; Vear, 2005).

Our approach to mapping and examining the history of sedimentary flux to the Mauritanian basin builds on these observations and has three steps. First, we map basin stratigraphy using two-dimensional seismic and well data, provided courtesy of Tullow Oil Plc. and TGS. Second, the distribution of sedimentary rock in the basin is used to calculate histories of sedimentary flux. Finally, we invert 14,700 longitudinal river profiles from across the African continent for a Cenozoic history of uplift. These results are combined with measured solid sedimentary flux at Africa's major deltas to examine the relationship between subplate support, sediment routing, and deposition of clastic material at Africa's passive margins. We show that combining uplift histories calculated by inverting river profiles with calculated incision and sedimentary flux histories and stratigraphic mapping offshore provides a link between sediment sources and sinks at continental scales.

2. Data

2.1. Well Data

Eight commercial wells and one International Ocean Discovery Program well were used to map stratigraphy and provide biostratigraphic age constraints. The wells are located in the north, center, and south of the basin and are summarized in Table 1. Planktonic foraminiferal and calcareous nannoplankton assemblages have been calibrated using standard N and CN schemes (Table 2). The deepest well penetrated > 4 km of Recent to Cretaceous stratigraphy (Figure 3).

2.2. Seismic and Check-Shot Data

Stratigraphy was mapped across the margin by combining well data with 38 two-dimensional seismic lines from the TGS "Dolphin" survey, which had a 10×5-km grid spacing and record lengths of 8- to 10-s two-way time. Figures 4a–4d show seismic data from the northern and southern portions of the Mauritanian basin, and Figures 4e and 4f show a strike line that extends from the south to the north of the basin. The quality and resolution of the seismic data are generally very good and only deteriorate beneath salt structures. A seismic dip line that extends across the center of the Mauritanian basin is also shown in Lodhia et al. (2018). Seven prominent acoustic impedance anomalies were identified as seismic marker horizons and mapped across the data set. Well data are used to determine the age of these marker horizons (seabed, 5.6, 23.8, 58.4, 70.4, and 89.4 Ma, and acoustic basement; Figure 3). A regional chronostratigraphy of the Mauritanian basin

Table 2
Biostratigraphy of Seismic Horizons Identified at Wells in This Study

Horizon (age, Ma)	Type	Occurrence	Species	Abbreviation	Biostratigraphic range	Well	Reference
5.6	**PF**	**FO**	***Globorotalia tumida***	*G. tum.*	**Present-Messinian**	**E**	Wade et al. (2011)
11.4	PF	LO	*Globorotalia mayeri*	*G. may.*	Mid. Miocene-Mid. Oligocene	G, C, F	Bolli et al. (1989)
12.7	PF	FO	*Globorotalia praefohsi*	*G. prae.*	Mid. Miocene	C, F	Blow (1969), Kennett and Srinivasan (1983), and Wade et al. (2011)
15.1	PF	FO	*Orbunia sp.*	*Orb. sp.*	Holocene-Miocene	C, F	Young et al. (2018)
23.8	**PF**	**FO**	***Globorotalia kugleri***	*G. kug.*	**Early Miocene**	**E, G**	Blow (1969) and Berggren et al. (1995)
29.0	PF	LO	*Globigerina increbescens*	*G. inc.*	E. Oligicene-Mid. Eocene	G	Bandy (1949), Blow (1979), and Leckie et al. (1993)
45.7	PF	FO	*Turborotalia griffinae*	*T. grif.*	Eocene	D	Olsson et al. (2006)
53.7	CN	FO	*Sphenolithus editus*	*S. edit.*	Early Eocene	B	Perch-Nielsen et al. (1978)
58.4	**CN**	**FO**	***Fasciculithus bitectus***	*F. bit.*	**Paleocene**	**H**	Romein (1979) and Monechi et al. (2013)
58.4	**PF**	**LO**	***Globanomalina pseudomenardii***	*G. psdm.*	**Paleocene**	**A**	Bolli, (1957, 1957) and Olsson et al. (1999)
58.4	**CN**	**LO**	***Cruciplacolithus tenuis***	*C. ten.*	**Paleocene**	**B**	Perch-Nielsen (1977) and Varol (1989)
62.3	PF	FO	*Globigerina angulata*	*G. ang.*	Paleocene	A	Olsson et al. (1999)
70.4	**CN**	**LO**	***Tranolithus phacelosus***	*T. phac.*	**Cretaceous**	**B**	Brown et al. (1998) and Burnett (1998)
75.9	CN	LO	*Lithastrinus grilli*	*L. gril.*	Late Cretaceous	B	Burnett (1998)
78.0	PS	FO	*Rosita fornicata*	*R. forn.*	Cretaceous	A	Plummer (1931)
81.3	CN	LO	*Bukryaster hayi*	*B. hayi*	Late Cretaceous	B	Burnett (1998)
84.9	CN	LO	*Lithastrinus moratus*	*L. mor.*	Late Cretaceous	B	Burnett (1998)
89.0	**CN**	**FO**	***Marthasterites furcatus***	*M. fur.*	**Late Cretaceous**	**B**	Bolli et al. (1989) and Burnett (1998)
89.0	**PS**	**LO**	***Triorites africaensis***	*T. afr.*	**Cretaceous**	**A**	Jardiné and Magloire (1965)
94.0	CN	LO	*Rotalipora cushmani*	*R. cush.*	Cretaceous	B	Sigal (1948)
139.4	CN	LO	U. gr. granulosa	*U. gr. gr.*	Cretaceous-Jurassic	B	Bralower et al. (1989)

Note. Seismic horizons in bold are correlated across the basin (Figures 3 and 4), depth converted and decompacted (Figure 6) to calculate solid sedimentary flux (Figure 7). PF = planktonic foraminifera, CN = calcareous nannofossil, PS = palynofossil, FO = first occurrence, LO = last occurrence.

produced using seismic and well data is shown in Figure 5. Ages of hydrocarbon source rock and reservoir intervals are from Vear (2005) and Davison (2005).

2.3. Continental Drainage and Dynamic Topography

A digital elevation model (DEM) of the African continent was generated using the 3-arcsecond Shuttle Radar Topography Mission data set, which has a resolution of $\sim 90 \times 90$ m (Farr et al., 2007). Hancock et al. (2006) tested the vertical and horizontal accuracy Shuttle Radar Topography Mission data by benchmarking against GPS measurements on spatial scales of 10^1–10^6 m, yielding values of $\pm$16 and $\pm$20 m, respectively. In order to extract longitudinal river profiles, anomalous spikes and sinks were first removed from the DEM. Flow routing algorithms in the Esri software package, ArcGIS, were used to identify the direction of steepest descent. The number of cells upstream of any given cell was calculated, and a threshold drainage area (4 km^2) determined the minimum number of cells which contribute to the initiation of overland flow. A total of 14,700 rivers has been extracted from the DEM and verified using LandSat satellite imagery (Figure 1).

3. Methodology

3.1. Solid Sedimentary Flux

3.1.1. Regional Velocity Model and Depth Conversion

All wells are approximately vertical (i.e., they have minimal horizontal deviations) and have time-depth (check shot) measurements that are broadly similar. These observations suggest that a one-dimensional

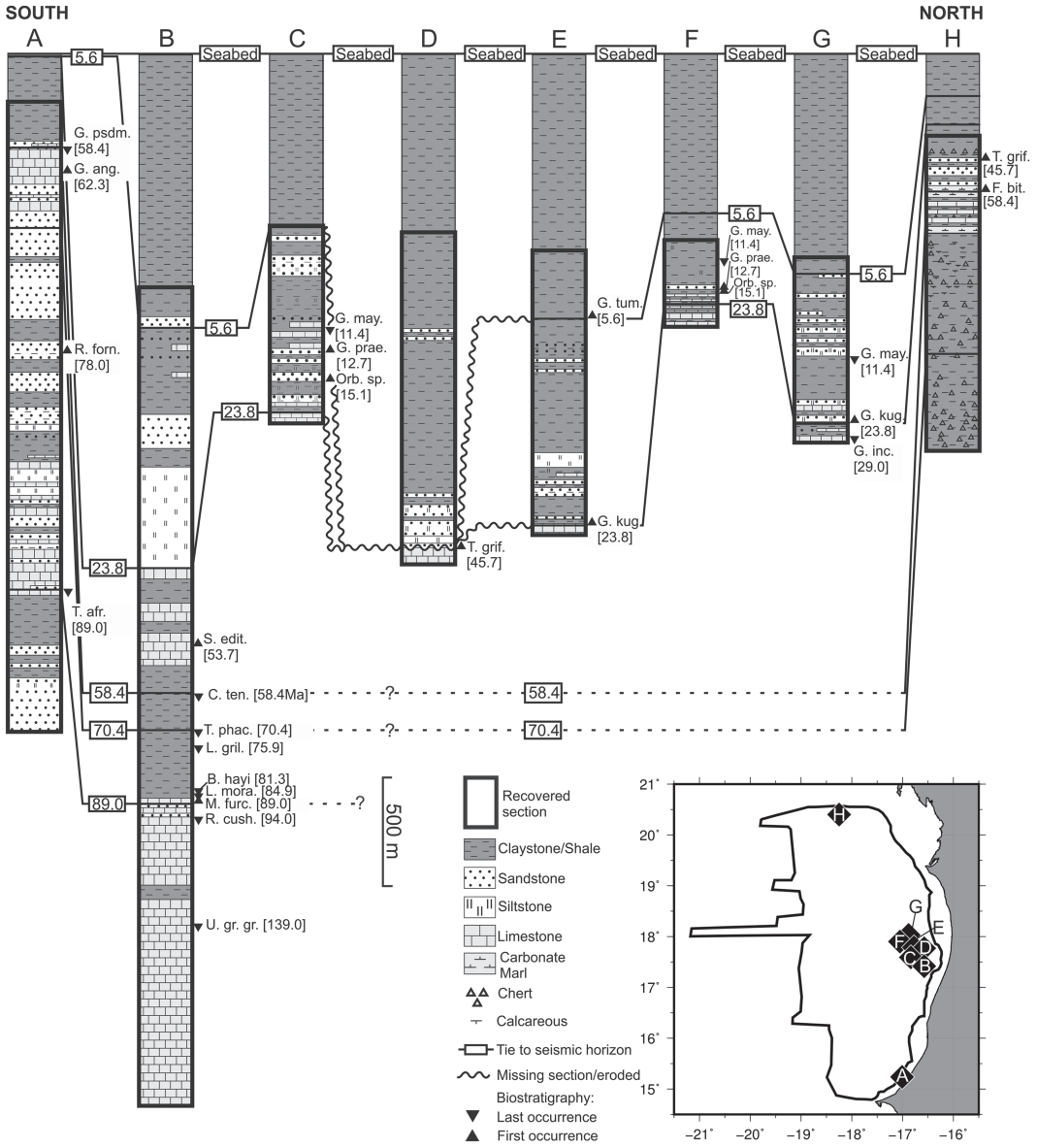


Figure 3. Mauritanian stratigraphy. Correlation of stratigraphy recorded in wells. Biostratigraphy including first and last occurrences and age are abbreviated in this figure and described in Table 2. Inset map shows location of wells (see Figure 2d).

velocity model is probably appropriate. Mean time-depth values were used to generate a velocity model that has the form $z(t) = 0.0017t^2 + 0.9t - 34$, where t = two-way travel time in milliseconds. The velocity model, extrapolated at depths > 4.5 km, is shown in Figure 6 (see supporting information). We acknowledge that more complete velocity models could be used to improve accuracy of depth conversion along the margin. Stratigraphic horizons were interpolated between the depth-converted seismic lines and wells using continuous curvature splines (Smith & Wessel, 1990; supporting information). One standard deviation of observed time-depth pairs from all wells and a range of compaction parameters were propagated through depth conversion and decompaction calculations to estimate uncertainties in solid sedimentary flux.

3.1.1. Compaction Parametrization and Decompaction

In order to calculate solid sedimentary flux, we must first correct for compaction caused by sedimentary loading. Porosity, ϕ, was parameterized using Athy, 's (1930) formulation,

$$\phi = \phi_\circ \exp\left(-\frac{z}{\lambda}\right). \quad (1)$$

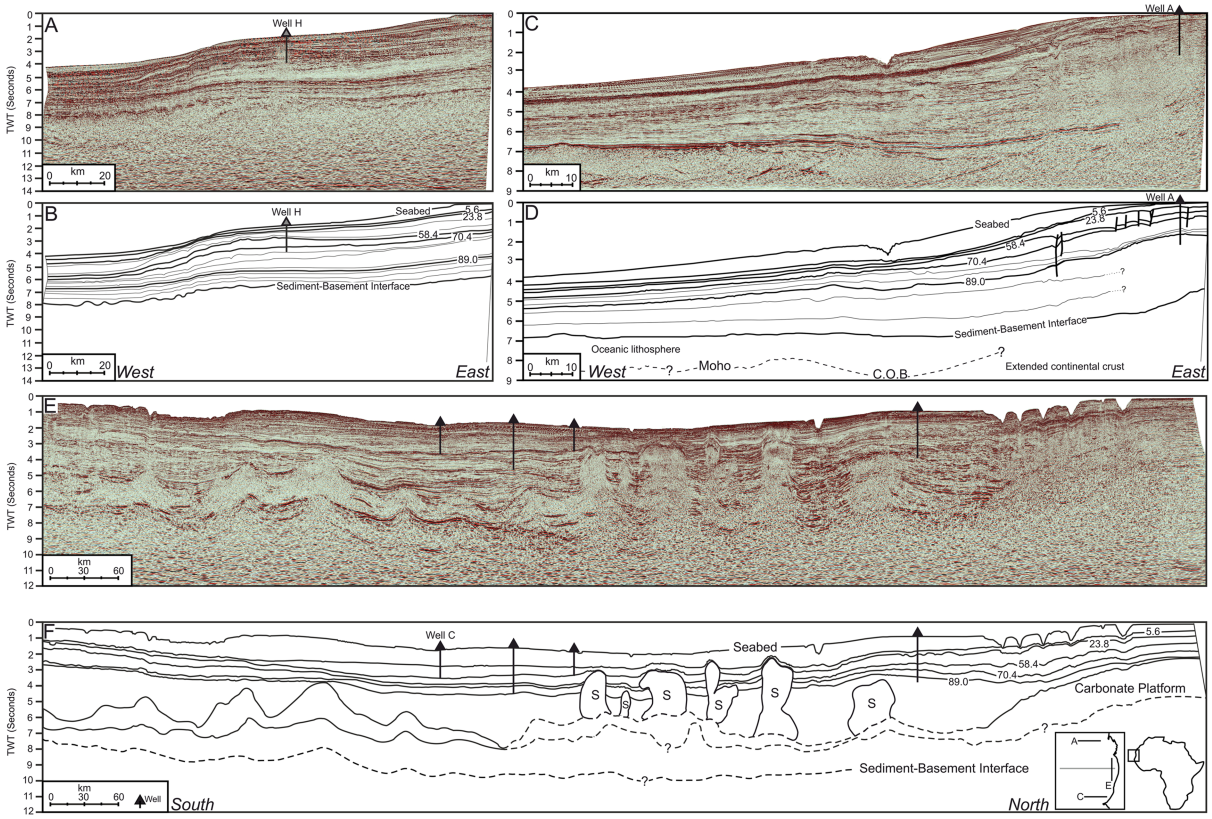


Figure 4. Seismic data. (a, b) Northern seismic line and interpretation. (c, d) Southern seismic line and interpretation. (e, f) South-North strike line in the center of the Mauritanian basin and interpretation. Imagery is generally excellent away from salt. Unlabeled black triangles = positions of additional nearby wells in the Mauritanian basin projected onto South-North strike line. Black lines labeled on inset map = positions of seismic lines in this study. Gray line on inset map = location of seismic dip line shown in Lodhia et al. (2018). Seismic data provided courtesy of TGS.

The initial porosity, $\phi_\circ$, and compaction wavelength, λ, were constrained as follows. First, a simple relationship between velocity as a function of depth, $v(z)$, and compaction, was assumed such that

$$\frac{1}{v(z)} = \frac{\phi(z)}{v_w} + \frac{1-\phi(z)}{v_{sg}}, \tag{2}$$

where v_w is pore fluid velocity and v_{sg} is solid grain velocity (Wyllie et al., 1956). For seawater, $v_w = 1.5$ km/s. We assume that $v_{sg} = 5.5 \pm 0.5$ km/s, which is appropriate for a mixture of sand and clay (Christensen, 1982). Since two-way time, $t = 2\int_0^z dz/v(z)$, we can combine equations (1) and (2) to obtain

$$\frac{t}{2} = \frac{z}{v_{sg}} + \phi_\circ \lambda \left(\frac{1}{v_w} - \frac{1}{v_{sg}}\right)\left[1 - \exp\left(-\frac{z}{\lambda}\right)\right]. \tag{3}$$

We seek the minimum root-mean-square (rms) misfit between observed and theoretical time-depth values by varying $\phi_\circ$ and λ, such that we minimize

$$\text{rms} = \sqrt{\frac{1}{N}\sum_{i=1}^{N}\left(t_o^i - t_c^i\right)^2}, \tag{4}$$

where t_o and t_c are observed and calculated times. N is the number of time-depth measurements (Figure 6).

We remove the effects of loading (i.e., decompact) and calculate the solid thickness of a sedimentary layer, T_{sol}, such that

$$T_{sol} = z_2 - z_1 + \phi_\circ \lambda \left[\exp\left(-\frac{z_2}{\lambda}\right) - \exp\left(-\frac{z_1}{\lambda}\right)\right], \tag{5}$$

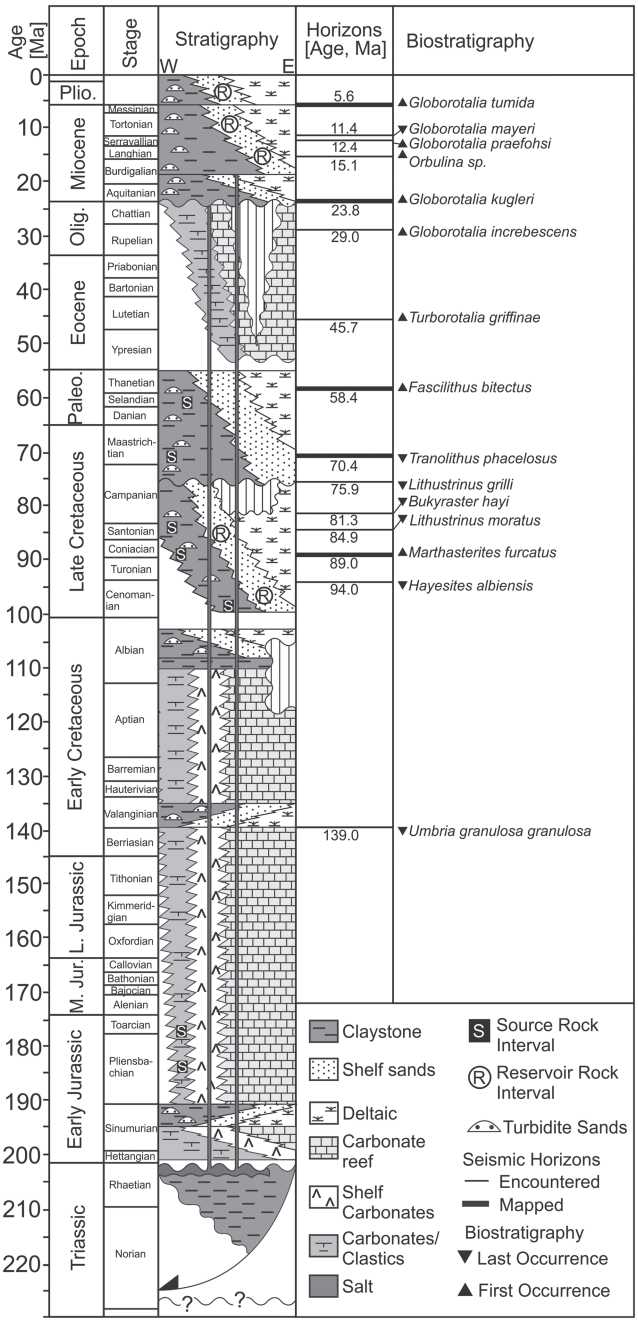


Figure 5. Mauritanian chronostratigraphy and biostratigraphy. Up/down arrows = first/last occurrences of planktonic foraminifera, calcareous nannofossils, and palynofossils used to constrain ages of seismic horizons across the Mauritanian margin.

which corrects for the effects of compaction. We used the compaction parameters, $\phi_\circ = 0.75 \pm 0.1$, $\lambda = 2.66 \pm 1.2$ km, that best fit the mean time-depth pairs of all check-shot data in our selected wells (Figure 6). z_1 and z_2 are the depths of the top and bottom of a seismic interval, respectively (e.g., Walford et al., 2005). Solid sedimentary thickness of rock in the Mauritanian basin is shown in Figure 7. Solid sedimentary fluxes are summarized in Table 3 and are shown in Figures 7 and 8 (see supporting information).

3.2. Inverse Modeling of Drainage

To investigate the source of sedimentary flux to Africa's passive margins, we began by inverting the drainage inventory for a history of Cenozoic uplift rates. First, a suitable forward model has to be defined. The rate of

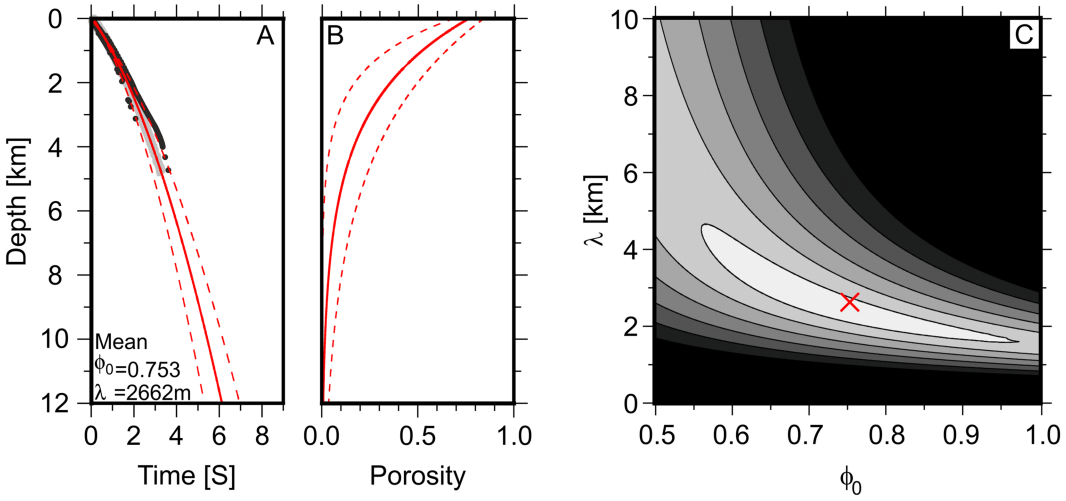


Figure 6. Depth conversion and compaction. (a) Black circles = check-shot data for wells on the Mauritania margin (see Figure 2d; (Lodhia et al., 2018)). Best fitting compaction parameters (initial porosity, $\phi_\circ$, and compaction wavelength, λ) were determined by minimizing misfit between mean of observed check-shot data (gray curve) and calculated time-depth curves. Best fitting time-depth curve (solid red line) was generated using compaction parameters shown by red cross in panel (c) and solid red curve in panel (b). Dashed red curves = one standard deviation from the mean time-depth curve. (b) Solid red curve = best fitting porosity, ϕ, as a function of depth, z. Dashed red curves = one standard deviation from the mean compaction curve. (c) Compaction parametrization. Root-mean-square misfit between observed mean and calculated time-depth curves plotted as a function of initial porosity and compaction wavelength. Red cross = compaction parameters with lowest residual misfit to time-depth data (solid red curve in panel a).

change of elevation, $\partial z/\partial t$, of a river must be a function of uplift rate, U, and erosion rate, E

$$\frac{\partial z}{\partial t} = U(x,t) - E(x,t), \tag{6}$$

where x is the downstream distance from the river source and t is time. The erosion rate, $E(x,t)$, parameterizes a complex suite of fluvial erosional processes. It is generally accepted that the stream power model provides a pragmatic way of modeling drainage patterns at long length and time scales and can be expressed in a simple form as

$$E(x,t) = vA(x)^m \left(\frac{\partial z}{\partial x}\right)^n, \tag{7}$$

Table 3
Solid Sedimentary Flux of the Mauritanian Basin

Time (Ma)	Rate	Error
0–5.6	1.90	+2.00/−1.40
5.6–23.8	0.20	+0.20/−0.10
23.8–58.4	0.16	+0.18/−0.11
58.4–70.4	0.25	+0.21/−0.17
70.4–89.0	0.41	+0.21/−0.18
89.0–225	0.51	+0.15/−0.13

Note. Solid flux was calculated using the volume of solid sedimentary rock between seismic intervals mapped across the basin (Figures 4 and 7). Rate and its uncertainty have units of 10^3 km^3/Ma. Errors for solid sedimentary flux are calculated by propagating compaction parametrization uncertainties. A tentative age of ~225 Ma is assigned to the basement, based on the age of Gondwana breakup (see, e.g., Brownfield & Charpentier, 2003; Davison, 2005; Vear, 2005).

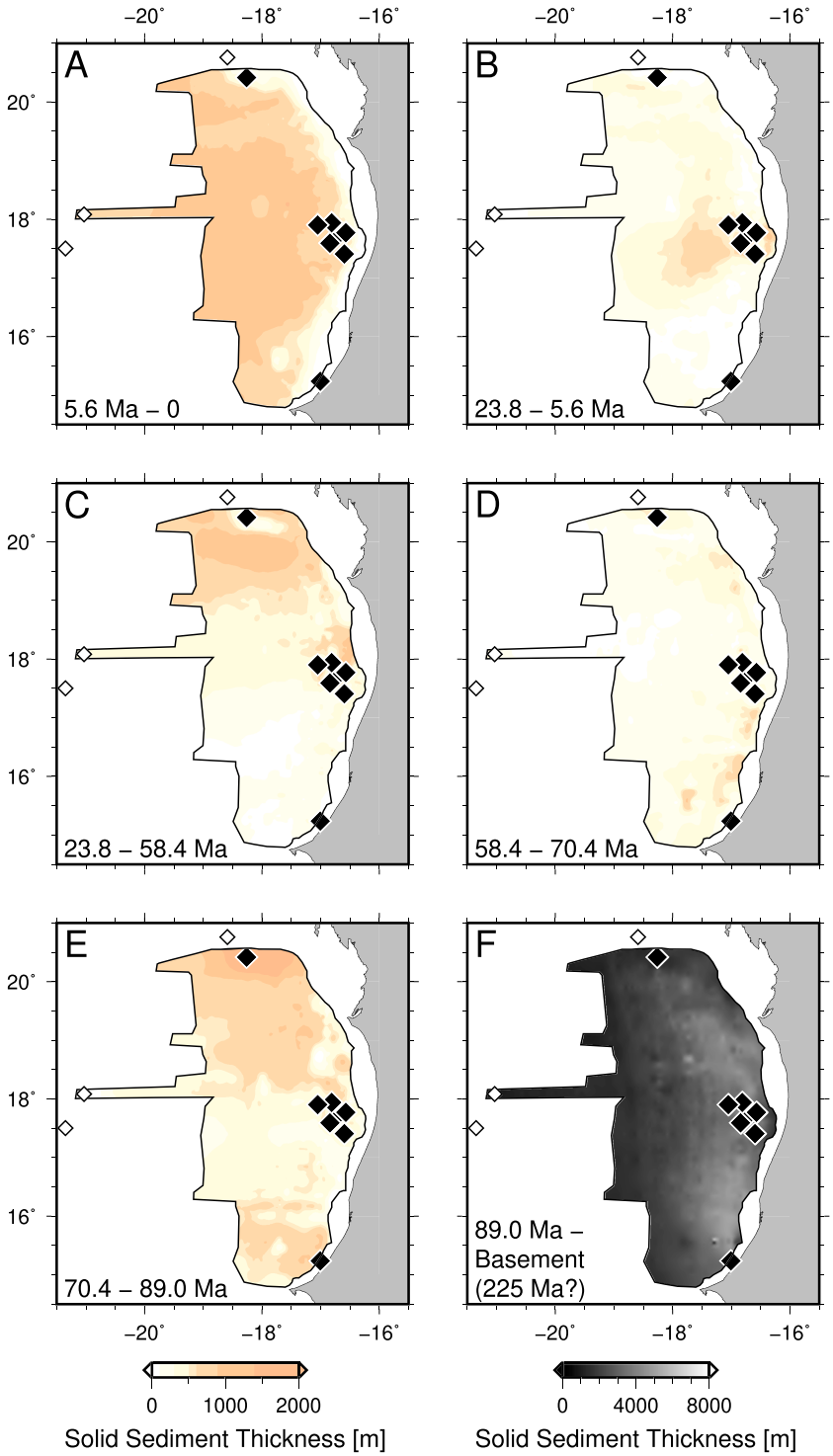


Figure 7. Solid sedimentary thickness. (a–f) Thickness of solid sedimentary rock between seismic horizons identified in Mauritanian basin (Figures 4 and 5). Black/white diamonds = exploration/Deep Sea Drilling Project (DSDP) and Ocean Discovery Program (ODP) wells; black polygon = boundary of seismic dataset. Note that panel f, which shows the interval between acoustic basement (~225 Ma) and 89 Ma, has a color scale with a larger range than panels a–e.

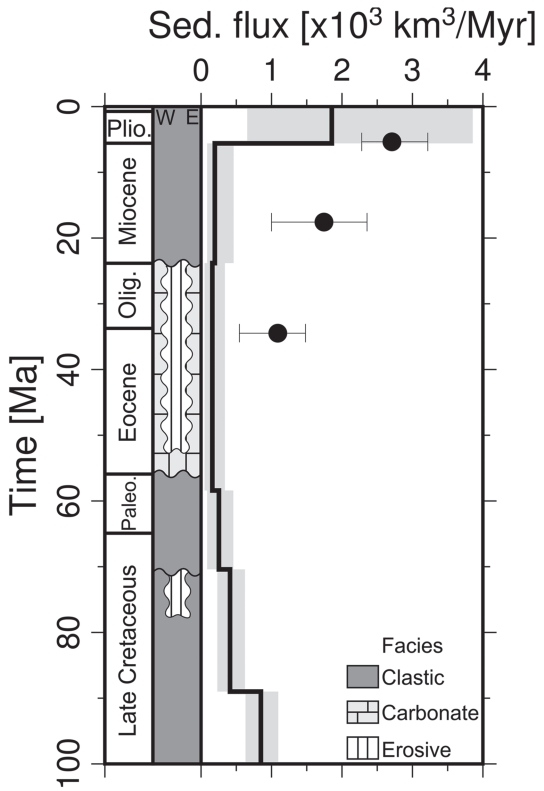


Figure 8. Mauritanian solid sedimentary flux. Black lines and gray polygon = solid sedimentary flux and uncertainties calculated from compaction parameters (see Table 3). Black circles with error bars = sedimentary flux of Sene-Gambia calculated from estimates of denudation in sub-Saharan West Africa (Grimaud et al., 2018). Left panel shows simplified Mauritanian chronostratigraphy; see Figure 5.

where v is a calibration constant with the dimensions of velocity if $m = 0$ and $n = 1$. A is upstream drainage area, which can be measured at the present day (e.g., Crosby & Whipple, 2006; Hack, 1957; Howard, 1971, 1988; Howard & Hemberger, 1991, 1987; Howard & Kerby, 1983; Howard et al., 1994; Pritchard et al., 2009; Roberts & White, 2010; Roberts et al., 2012a, 2012b; Rosenbloom & Anderson, 1994; Rudge et al., 2015; Sklar & Dietrich, 1998, 2001; Tomkin et al., 2003; Weissel & Seidl, 1998; Whipple & Tucker, 1999; Whittaker et al., 2007; Whittaker & Boulton, 2012). The erosional parameters v, m, and n affect shapes of predicted river profiles in different ways (e.g., Pritchard et al., 2009; Roberts & White, 2010; Roberts et al., 2012a; Rosenbloom & Anderson, 1994; Whipple & Tucker, 1999). There is considerable debate about the values of v, m, and in particular n (e.g., Lague, 2014; Mudd et al., 2014; Van der Beek & Bishop, 2003). It has been shown that v and m trade off negatively with each other so that different combinations of v and m yield equally acceptable fits between observed and calculated river profiles (Croissant & Braun, 2014; Roberts & White, 2010). If $n \neq 1$, shocks can occur, whereby steeper slopes propagate faster than shallower slopes (Pritchard et al., 2009; Royden & Perron, 2013). We have no compelling evidence for shock wave behavior along rivers at the long wavelengths of which we are concerned. Fits between observed and theoretical river profiles are lowest when $n \sim 1$ (see Paul et al., 2014) which is corroborated by some field studies (Whittaker et al., 2007; Whittaker & Boulton, 2012). v must be calibrated using independent geological data. The value of m depends to some extent on the topology of the drainage network. Its value can be estimated by comparing misfit between families of observed and theoretical river profiles generated by a systematic sweep of parameter values. Paul et al. (2014) and Rudge et al. (2015) calibrated erosional parameter values in Africa and give us a basis for setting $v = 3.62$, $m = 0.35$, and $n = 1$.

Pritchard et al. (2009) and Roberts and White (2010) developed linear and nonlinear inverse approaches to calculate uplift rate histories from African river profiles. Their results indicate that at long wavelengths the erosional process appears to be dominated by advection, for example, knickpoint retreat. Changes in lithology and discharge appear to play moderating roles in determining the transient form of African river profiles (see, e.g., Roberts et al., 2019). The calculated uplift rate histories of African domes (e.g., Bié, Southern

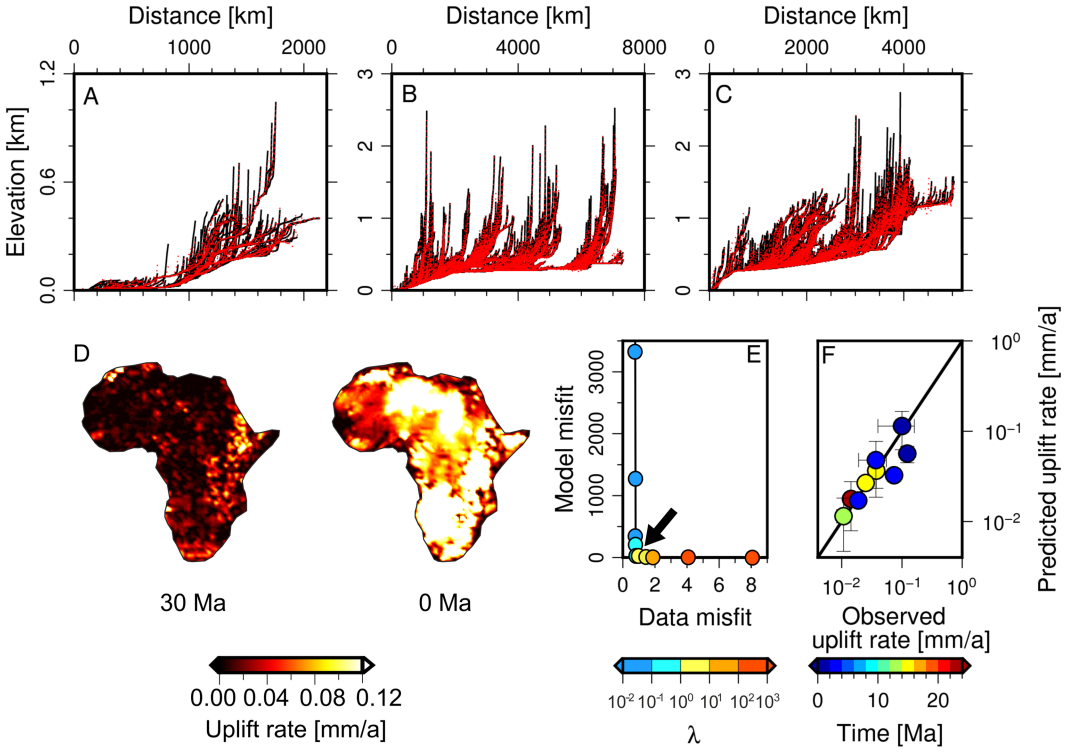


Figure 9. Inverting African drainage inventory. (a–c) Observed (black) and best fitting (red) theoretical river profiles for three major African catchments: (a) Senegal, (b) Niger-Chad, (c) Congo. Best fitting profiles were generated from uplift history shown in Figure 10. (d) Calculated uplift rates at 30 and 0 Ma. (e) Data misfit as function of spatial smoothing for series of inverse models. Colored circles = residual misfit for a suite of inverse models run with different values of smoothing parameter λ_S (e.g., Rudge et al., 2015). Black arrow = optimal (i.e., smoothest best fitting) model used to generate uplift history shown in panel d and Figure 10. Residual root-mean-square misfit for optimal inverse model = 0.81. (f) Comparison of independent and calculated uplift rates (see Rudge et al., 2015, for compilation; Figure 10a). Circles = weighted mean values of uplift rate where color indicates age. Vertical/horizontal lines = uncertainties calculated using methodology described in Rudge et al. (2015).

Africa) indicate that these swells grew during the last 40–30 Ma at rates of fractions of a millimeter per year, which is broadly consistent with independent geologic observations (see, e.g., Rudge et al., 2015). Roberts et al. (2012a) generalized this approach to solve for uplift rate as a function of space and time. They showed that families of longitudinal river profiles contain coherent information about histories of regional uplift. Paul et al. (2014) extracted and inverted 710 river profiles of Strahler order ≥ 5, to calculate an uplift rate history of Africa since 50 Ma. Rudge et al. (2015) subsequently showed that similar results can be obtained by linear inversion, which greatly speeds up the inversion process. Other similar inversion schemes exist (e.g., Croissant & Braun, 2014; Goren et al., 2014).

In this study, we use an inventory of 14,700 rivers to invert for an uplift rate history of the African continent during the last 30 Ma using the approach described in Rudge et al. (2015). In this scheme a linear version of the kinematic wave equation (equation (7) with $n = 1$) is solved using the method of characteristics. Elevations, z, of theoretical longitudinal river profiles

$$z = \int_0^{\tau_G} U(x(t), t)\mathrm{d}t, \quad \text{where} \quad \tau_G = \int_0^x \frac{\mathrm{d}x}{vA^m}. \tag{8}$$

The resultant matrix equation has the form $\mathbf{z} = M\mathbf{U}$. Since this problem can be underdetermined a damped least squares approach is used to invert the drainage inventory for a history of uplift by minimizing

$$|M\mathbf{U} - \mathbf{z}|^2 + \lambda_S^2|S\mathbf{U}|^2 + \lambda_T^2|T\mathbf{U}|^2, \quad \text{subject to} \quad \mathbf{U} \geq 0. \tag{9}$$

The matrices S and T represent spatial and temporal smoothing. Parameters λ_S and λ_T control the smoothness of calculated uplift histories. We sought the smoothest model that best fit the data by systematically

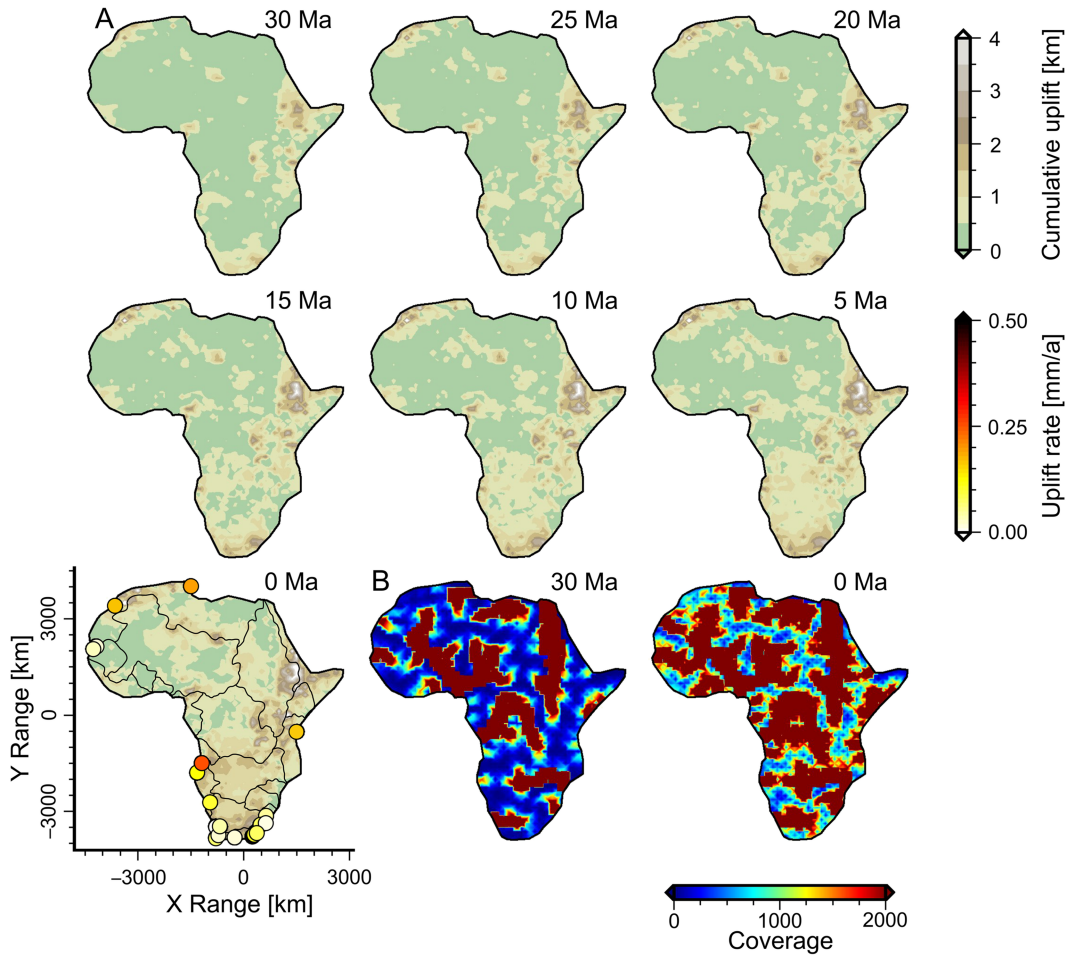


Figure 10. Calculated uplift history. (a) Calculated spatial and temporal pattern of cumulative uplift from inversion of 14,700 river profiles. Black curves in 0-Ma panel = present-day African drainage divides; colored circles = independently determined uplift rates used to test calculated uplift history (see Figure 9f). (b) Model coverage (nullity) plots showing number of nonzero entries in model matrix (see body text).

varying damping parameters (Figure 9e; Rudge et al., 2015). In this study, $\lambda_S = 0.1$ and $\lambda_T = 0$. We assume that drainage planform remains constant, which is consistent with interpretations of incised deeply weathered surfaces in northwest Africa (see Chardon et al., 2016). We also assume that incision as a result of sea level drop (e.g., Messinian Mediterranean sea level fall) occurred on sufficiently rapid time scales ($\lesssim$ 5 Ma) that they have not affected the longitudinal shapes of modern drainage networks (see, e.g., Loget et al., 2006). It is then straightforward to solve for incision rates (e.g., Stephenson et al., 2014).

It is important to acknowledge that model resolution (coverage; number of nonzero entries in model matrix M) decreases further back in time as fewer rivers constrain older uplift histories (Figure 10b; Rudge et al., 2015). Figure 10 shows calculated cumulative uplift (i.e., $\int U\mathrm{d}t$) and model coverage, which indicates that calculated uplift is well resolved across most of Africa since ~30 Ma (see Rudge et al., 2015).

3.3. Predicting Sedimentary Flux From Drainage Patterns

Sedimentary flux can be predicted by integrating incision rates with respect to distance downstream. For example, if we assume that $n = 1$ and that erosion diffusivity is negligible, sedimentary efflux, Q_s, as a function of time, can be predicted at the mouth of a river, such that

$$Q_s(t) = -v \int_{\circ}^{L} A(x)^m \frac{\partial z}{\partial x} \mathrm{d}x, \tag{10}$$

where L is the length of the river. We note that solving this integral yields flux with units of area per time, which can be converted into an estimate of volumetric flux using information about river widths. Due to a

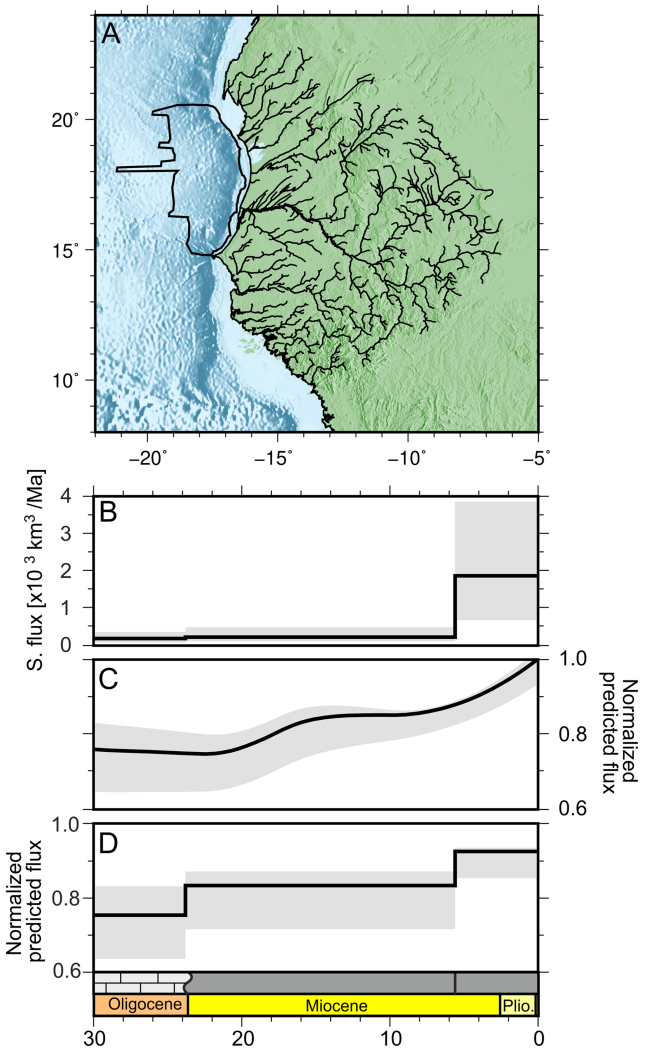


Figure 11. A qualitative comparison of observed and simulated sedimentary flux histories. (a) West African drainage extracted from Shuttle Radar Topography Mission digital elevation model. Black polygon = extent of mapped seismic data in Mauritanian basin. (b) Solid sedimentary flux measured from wells and seismic data offshore (see Figures 7 and 8). (c) Normalized, predicted sedimentary flux calculated using the best fitting uplift history shown in Figure 10 and a simple stream power formulation of fluvial erosion (see body text). (d) Average predicted sedimentary flux between 23.8, 5.9, and 0 Ma (i.e., at the resolution of mapped stratigraphy); gray band = calculated sedimentary flux for ±50% drainage area.

lack of information about river widths through time, predicted solid sedimentary flux was normalized using maximum calculated values (Figure 11). Our approach to estimating sedimentary flux has three steps. First, a finite-difference scheme was used to calculate incision rate at each position in the drainage inventory (see Roberts & White, 2010). This model was parameterized using the uplift history shown in Figure 10a. Second, we integrated calculated incision rates along the Senegal river and other major rivers disgorging into the Atlantic Ocean atop the Mauritanian basin. Finally, predicted flux was binned so that it had the same temporal resolution as measured offshore flux and its value normalized by maximum calculated flux. This approach provides a way to link uplift, erosion, and sedimentary flux in a deterministic framework, which can be tested using independent observations of solid sedimentary flux.

4. Results

4.1. Stratigraphy

Up to 8 km of sedimentary rock is present between the acoustic basement and the oldest, biostratigraphically dated, basin-wide seismic horizon (89 Ma; Turonian) in the Mauritanian basin (Figure 7f). The extent

of the Mauritanian salt and underlying rift basins can be seen clearly in the seismic data and covers parts of the study area (Figures 4e–4f). The earliest phase of Atlantic margin deposition in northwest Africa is recorded by red-bed sandstones, typical of an arid continental environment, which dominate the Triassic section in the Essaouira Basin of Morocco (Vear, 2005). In common with previous authors, we assume a Late Triassic (~225 Ma) age for the acoustic basement based on Moroccan analogs to the north of the Mauritanian basin (e.g., Brownfield & Charpentier, 2003; Davison, 2005; Vear, 2005). All known intersections of salt within the MSGBC Basin (Casamance-1, Maritime-3, 5, 8 in Senegal and Chinguetti-1 in Mauritania) are allochthonous (Vear, 2005). There are no reported intersections of synrift evaporites in any wells in the MSGBC Basin. However, analogs of synrift evaporites deposited during the later stages of rifting in the Proto-Central Atlantic ocean in the axes of the Triassic-Early Jurassic graben are recovered north of the MSGBC Basin along the northwest African margin in Morocco. Therefore, we assume an Early Jurassic age for synrift salt deposition in the MSGBC Basin (Brownfield & Charpentier, 2003; Davison, 2005; Emery & Uchupi, 1984; Vear, 2005). In the Essaouira Basin of Morocco the most complete stratigraphy was encountered in well JRP-1 (see Figure 6b in Davison, 2005). Central Atlantic Magmatic Province basalts have been found below, within, and above the Triassic evaporite sequence (see Figure 6b in Hafid et al., 2000), which indicates that the age of the salt is 200 ± 1 Ma (Early Jurassic; Davison, 2005).

The oldest, dated horizon in the Mauritanian basin is 139.0 Ma, which was sampled at a depth of ~4.2 km in Well B (Figure 3). Upper Jurassic-Albian stratigraphy is dominated by platform carbonates (limestones), which are visible on seismic data and extend across the continental margin of the basin (Figure 4). Upper Cretaceous-Paleocene stratigraphy in the center of the basin is almost exclusively clastic (e.g., claystones, shale, siltstones, and sandstones), whereas ~500 m of limestone was encountered at Well A, to the south. Almost all of the rocks between the 58.4 and 23.8 Ma (Eocene-Miocene) marker horizons are carbonate. Increased incision along the continental margin is observed in the center of the basin at Well D where the majority of Oligocene-Eocene stratigraphy has been removed. Importantly, Miocene-Recent clastic stratigraphy encountered at all wells consists of sandstones and claystones/shale on the continental shelf and basin floor, respectively. Rock recovered from the upper sections (100–1,000 m) of all wells is characterized by unconsolidated claystones and shales with high porosity.

4.2. Solid Sedimentary Flux of the Mauritanian Basin

Stratigraphic mapping, depth conversion, and decompaction indicate that solid sedimentary flux decreased from $0.41^{+0.21}_{-0.18} \times 10^3$ km^3/Ma during the Cretaceous, to Paleocene rates of $0.25^{+0.21}_{-0.17} \times 10^3$ km^3/Ma and Oligocene rates of $0.16^{+0.18}_{-0.11} \times 10^3$ km^3/Ma. Uncertainties were calculated by propagating depth conversion and compaction errors. Volumes of mapped carbonate indicate that Eocene-Oligocene clastic flux is approximately a factor of 2 smaller than these values. The distribution of sedimentary rock varies significantly with time. Late Cretaceous deposition (Figure 7e) is concentrated at the northern and southern parts of the basin and was followed by low Paleocene rates of deposition across the basin (Figure 7d). Eocene-Oligocene deposition was concentrated in the northern part of the basin.

About 1.5 km of 23.8- to 5.6-Ma clastic rock was deposited in the center of the basin. Up to 2 km of sediment was deposited across most of the basin from 5.6 to 0 Ma. Solid clastic sedimentary fluxes for the Miocene and post-Miocene are $0.2^{+0.20}_{-0.10} \times 10^3$ km^3/Ma and $1.9^{+2.00}_{-1.40} \times 10^3$ km^3/Ma, respectively. While the overall solid sedimentary flux during the Eocene-Oligocene is similar to that of the Miocene, it is important to note that the majority of Miocene sedimentation is restricted to a smaller region in the center of the basin adjacent to the Senegal river (Figure 7b). We note that these estimates of sedimentary flux are likely to be underestimates because we do not consider material that has gone into solution. To examine the origin of increased Neogene clastic flux, we inverted 14,700 longitudinal river profiles from across the African continent for a smooth history of uplift.

4.3. Calculated Uplift History of Africa

The residual misfit between observed and theoretical longitudinal river profiles is low (rms misfit = 0.81; Figures 9a–9c). Predicted uplift rates match those estimated from independent geologic constraints within error (e.g., uplift rates calculated from radiometric, cosmogenic and biostratigraphic dating of marine terraces and fluvial incision and correlation of oxygen isotope stages with marine terraces; Elmejdoub & Jedoui, 2009; Erlanger et al., 2012; Guiraud et al., 2010; Meghraoui et al., 1998; Partridge, 1998; Partridge & Maud, 1987, 2000; Roberts & Brink, 2002; see Rudge et al., 2015, for list of observed rates; Figures 9 and 10a). Model

coverage is greatest for the largest river systems and decreases with age. Calculated uplift rates were highest during the last 25 Ma (Figures 9d and 10a). There is significant growth of the Fouta-Djallon swell (West Africa), East African Rift system, and of domal swells in central and southern Africa. Calculated uplift of the Fouta-Djallon swell accelerated during the last ~5 Ma.

An important concern is that the planform of rivers (e.g., the Nile) might have changed, which could adversely affect the stability of calculated uplift histories. One way to examine this issue is by excising large catchments from the drainage inventory and reinverting the reduced data set (supporting information). These tests show that if, for example, the entire Nile catchment is removed, calculated cumulative uplift in other parts of the continent (e.g., the West African seaboard) differs from models run with the complete inventory by less than a few tens of meters (e.g., Figure 10). Moreover, we note that the erosional model used here raises drainage area to a small fractional power, which means that there can be large uncertainties, for example, $O(10)\%$, in upstream area without drastically altering calculated uplift rate or sedimentary flux histories (see, e.g., Figure 11).

5. Discussion

We discuss four results. First, we reexamine the stratigraphic history of northwest Africa's passive margin. Second, we discuss its punctuated history of sedimentary flux. Third, we explore how the sedimentary archive, uplift, and erosion of continental topography can be used to generate a Cenozoic source-to-sink framework for northwest Africa. Finally, we examine the implications of calculated sedimentary flux and uplift rate histories for evolution of African topographic support and mantle convection.

5.1. Northwest Africa's Passive Margin Stratigraphy

Jurassic to Lower Cretaceous-aged carbonates are intersected by several wells along the northwest African margin, including over 700 m of Berriasian lagoonal carbonates at Loup De Mer-1, MBour-1, Ndiass-1, and Dakar Marin-2 in Senegal (Vear, 2005). In addition, several wells intersect thick carbonates of this age in the Tarfaya and Aaiun Basins to the north in Morocco and Western Sahara, respectively (e.g., Cap Juby-1). A Jurassic carbonate shelf has also been identified on the conjugate Atlantic Seaboard of the United States (Vear, 2005).

With the exception of the northeast continental margin, Africa was separated from surrounding continents by Late Cretaceous times (e.g., Janssen et al., 1995). Cenomanian marine deposition is recorded onshore in northwest Morocco, northern and eastern African (e.g., Sahagian, 1988). High subsidence rates in the MSGBC and Gabon Basins during the Campanian-Maastrictian were probably generated by spreading between the central, equatorial, and southern sectors of the Atlantic ocean (Daly et al., 1989; Fairhead, 1988; 1988; Janssen et al., 1995). The lack of Late Cretaceous prograding clinoforms and clastic sedimentation recorded at Wells A, B, and H are probably partially related to rapid Cretaceous subsidence, which has been attributed to salt tectonics (Janssen et al., 1995). Carbonate deposition offshore broadly correlates with periods of predicted topographic quiescence onshore (i.e., low uplift rates). The pattern of decreasing solid sedimentary flux and increasing Paleogene carbonate production in the Mauritanian basin indicates that rates of continental clastic efflux were probably low. These observations are consistent with the distribution of indurated Paleoegene laterites and lateritic gravels onshore, which indicate that Cretaceous-Paleogene topographic gradients and physical erosion rates were also low (Burke & Gunnell, 2008; Grimaud et al., 2018; Ismail et al., 2010 Nyagah, 1995; Rouby et al., 2009; Salman & Abdula, 1995; Séranne & Nzé Abeigne, 1999). High sea level, intense inland weathering, and preferential deposition of phosphates and carbonates dominated the intercratonic and marginal basins of West Africa during the Paleocene-Eocene (Grimaud et al., 2018). Offshore deposition in the Mauritanian basin during this time is dominated by carbonates and erosion in the central part of the basin around Well D.

The base Miocene unconformity, 23.8 Ma, marks a significant change in sedimentation rate and facies in the Mauritanian basin. A major change from carbonate to clastic deposition is clearly seen across the entire basin from the Miocene until present day. Lodhia et al. (2018) show that 0.4–0.8 km of Neogene water-loaded subsidence is observed in the center of the Mauritanian basin. Subsidence histories, measured ocean-age depth residuals, magmatic histories, and shear wave tomographic modeling suggest that upper mantle convection has generated an east-west bathymetric gradient of ~1/300 between the Cape Verdé Rise and Mauritanian margin during the last ~23 Ma. This mantle convective drawdown generated 0.4–0.8 km of water-loaded accommodation space in the Mauritanian basin.

5.2. Sedimentary Flux: Clastic Versus Carbonate Deposition

An important question is what caused the change from carbonate to clastic sedimentation that occurred in the Mauritanian basin at ~ 23 Ma? Small increases in the delivery of clastic material to continental margins can greatly reduce the efficacy of carbonate production (e.g., Walker et al., 1983). In general, efflux rates vary between different drainage basins and are controlled by drainage area and relief and are moderated by other variables (e.g., climate; runoff; Milliman & Syvitski, 1992). The relatively high volumes of Miocene-Recent clastic rock mapped throughout the Mauritania basin indicate that delivery of clastic material to the margin increased by an order of magnitude. An obvious source of this clastic material is uplift and erosion of the continental hinterland. Grimaud et al. (2018) correlated relict lateritic landforms across northwest Africa to estimate Middle Eocene-Recent onshore denudation and sedimentary flux. They found that denuded volumes and offshore solid sediment accumulations are approximately balanced. They argue that the establishment of the modern Niger catchment must have occurred before 29 Ma, after which clastic material was provided to the Niger delta by growth of the dynamically supported Hoggar swell. Their calculated clastic efflux to the Sene-Gambia drainage basin follows the same trend which we observe in the Mauritanian basin further north, whereby solid sedimentary flux increases substantially from Eocene-Present times (Figure 8). Significant increases in solid sedimentary flux to the Sene-Gambia and Mauritanian basins occurred during the last ~5 Ma. From a tectonic point of view, it is surprising that uplift and clastic flux should increase so dramatically long after continental breakup has occurred. However, long wavelength free air gravity anomalies, positive residual ocean age-depth measurements, radial drainage patterns, and calculated histories of uplift indicate that the Fouta Djallon swell also grew (and was denuded) in response to regional subplate support during the last ~ 30 Ma.

5.3. A Source-to-Sink Framework From Inverting Drainage Patterns

Inversion of drainage patterns from across Africa suggest that this phase of clastic flux was accompanied and probably controlled by the acceleration in the growth of the Fouta Djallon and Atlas topographic swells (Figure 11). We examined whether stratigraphy offshore can be related to uplift histories onshore by inverting drainage networks and predicting sedimentary flux (equation (10)). Figure 11 shows that predicted sedimentary flux is broadly similar to that measured from stratigraphy in the Mauritanian basin. Increased Neogene clastic solid sedimentary flux to the center of the Mauritanian basin appears to be a response to post-Miocene uplift of the Atlas and Fouta-Djallon topographic swells. We note that the deposition of post-Miocene clastic sedimentary rock in the Mauritanian basin has led to the formation of important hydrocarbon reservoirs. In the future more complete landscape models could be parametrized using the calculated history of uplift to predict histories of volumetric sedimentary flux (e.g., Landlab: Hobley et al., 2017; Badlands: Salles et al., 2018).

5.4. Dynamic Support, Continental Uplift, and Offshore Sediment Deposition

Are changes in Neogene dynamic support and sedimentation observed in the Mauritanian basin observed elsewhere in Africa? It is widely accepted that Africa's domal swells have grown in response to mantle convective support during the last 30 Ma (Al-Hajri et al., 2009; Burke, 1996; Burke & Gunnell, 2008; Gurnis et al., 2000; Holmes, 1944; Moucha & Forte, 2011; Paul et al., 2014; Rudge et al., 2015). Results from inverse modeling of continental drainage patterns suggest that most swells grew steadily from 25 to 5 Ma and accelerated during the last 5 Ma (Figure 12). This pattern is seen across eastern, central, and southern Africa and is coeval with a Miocene change from carbonate to clastic sedimentation recorded at most major African deltas (e.g., Anka & Séranne, 2004; Nyagah, 1995; Paul et al., 2014; Reijers, 2011; Salman & Abdula, 1995; Sestini, 1989; Séranne & Nzé Abeigne, 1999). An increase in Oligocene to Neogene clastic flux is documented at many of Africa's major deltas (e.g., Nile, Jubba-Shebelle, Zambezi, Limpopo; Figure 12; Said et al., 2015; Walford et al., 2005). These observations are consistent with the notion that uplift, subsidence, and sedimentary flux to the Mauritanian margin are a manifestation of continent-wide, punctuated, Cenozoic dynamic support.

More broadly, our results suggest that periods of low continental uplift correspond with carbonate deposition at most deltas on Africa's passive margins. Widespread uplift of the African continent is concomitant with increased clastic sedimentary flux to most of its passive margins from Miocene-Recent times (Figure 11). Gravity anomalies, ocean age-depth residuals, tomography, and the history of magmatism indicate that uplift was driven by subplate support (e.g., Figure 2). These observations indicate that mantle convection plays an important role in determining stratigraphy and the distribution of hydrocarbon reservoirs around passive continental margins.

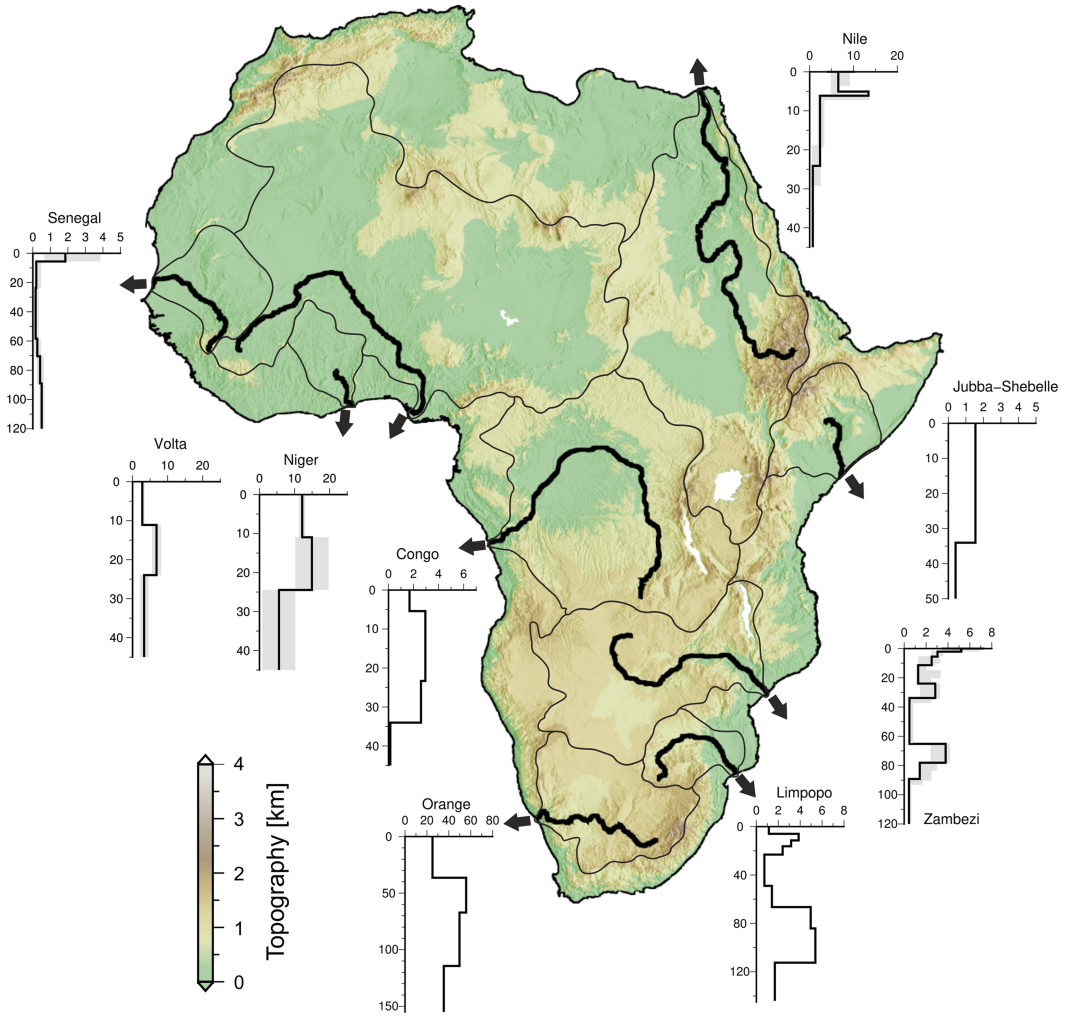


Figure 12. Continental sedimentary flux. Present-day topography, major drainage divides, and observed sedimentary flux of major African catchments. Sedimentary flux for Senegal is from this study; Volta: Paul et al. (2014); Niger: Grimaud et al. (2018); Congo: Paul et al. (2014); Nile: Aal et al. (2000), Hall et al. (2005); Jubba-Shebelle: DuToit et al. (1997); Zambezi: Walford et al. (2005); Limpopo: Dingle (1983); and Orange: Rust and Summerfield (1990), Rouby et al. (2009). Age on ordinate has units of mega-annum; sedimentary flux on abscissa has units of 10^3 km^3/Ma. Sedimentary flux histories plotted on a common timescale are shown in supporting information.

6. Conclusion

We examined Mesozoic to Recent sedimentary flux, uplift, and sedimentary routing histories of northwest Africa. Our results suggest that changing patterns of dynamic support generated flux of clastic material that is recorded by stratigraphy at its passive margins. We focus on calculating the history of solid sedimentary flux to the Mauritanian margin. Today, this region is fed by rivers draining the Atlas and Fouta Djallon topographic swells. Eight wells are combined with isopach mapping of seismic reflection data to constrain sedimentary flux since the breakup of Gondwana (~225 Ma). Calculated Late Cretaceous solid sedimentary flux was $0.41^{+0.21}_{-0.18} \times 10^3$ km^3/Ma, Paleocene flux was $0.25^{+0.21}_{-0.17} \times 10^3$ km^3/Ma, and Eocene-Oligocene flux was $0.16^{+0.18}_{-0.11} \times 10^3$ km^3/Ma. The distribution of offshore sedimentation in the Mauritanian basin varied significantly through time. Late Cretaceous sedimentary rock is concentrated at the northern and southern margins of the Mauritanian basin, while Paleocene sedimentary rock is distributed across the basin. Eocene-Oligocene sedimentary rock is thickest in the north of the basin. Extensive Early Cretaceous and Eocene-Oligocene carbonate platforms are mapped along the continental margin. A change from carbonate to clastic sedimentation occurred during Miocene times, and solid sedimentary flux increased

to $0.20^{+0.20}_{-0.10} \times 10^3$ km^3/Ma. Solid sedimentary flux increased again during Miocene to Recent times to $1.90^{+2.00}_{-1.40} \times 10^3$ km^3/Ma.

We investigate the source of clastic sedimentary flux to West Africa's passive margin by inverse and forward modeling of continental drainage patterns extracted from digital elevation data. Residual rms misfit between observed and theoretical longitudinal river profiles is low (rms = 0.81). Calculated uplift rates are corroborated by an independent inventory of uplift constraints from around Africa's coastline. We suggest that Neogene clastic flux to the Mauritanian margin was generated by denudation of the uplifting Atlas and Fouta-Djallon topographic swells from ~25 Ma, which appears to have accelerated during the last ~5 Ma. An increase in clastic sedimentary flux and concomitant change from carbonate to clastic offshore sedimentation is recorded at major African deltas, which we suggest was generated by increased Neogene uplift rates at many of Africa's domal swells. Inverse modeling of drainage patterns for uplift histories provides a deterministic methodology to link "sources" and "sinks" of sedimentary rock, which can help to predict the presence of offshore clastic and carbonate reservoirs generated as a response to hinterland evolution.

Acknowledgments
B. H. L. is supported by the National Environment Research Council Oil and Gas CDT studentship. We are grateful to Tullow Oil Plc. (www.tullowoil.com) and TGS (www.tgs.com) for providing access to seismic and well data. Requests for seismic and well data should be addressed to them. SRTM digital elevation data can be downloaded online (http://srtm.csi.cgiar.org). We thank three anonymous reviewers, V. Fernandes, R. Gawthorpe, H. Johnson, A. Lipp, G. Stucky de Quay, and J. Quye-Sawyer for their help.

References

Aal, A. A., El Barkooky, A., Gerrits, M., Meyer, H., Schwander, M., & Zaki, H. (2000). Tectonic evolution of the Eastern Mediterranean Basin and its significance for hydrocarbon prospectivity in the ultradeepwater of the Nile Delta. *The Leading Edge*, *19*(10), 1086–1102. https://doi.org/10.1190/1.1438485

Al-Hajri, Y., White, N., & Fishwick, S. (2009). Scales of transient convective support beneath Africa. *Geology*, *37*(10), 883–886. https://doi.org/10.1130/G25703A.1

Allen, P. A. (2008). Time scales of tectonic landscapes and their sediment routing systems. *Geological Society, London, Special Publications*, *296*(1), 7–28. https://doi.org/10.1144/SP296.2

Anka, Z., & Séranne, M. (2004). Reconnaissance study of the ancient Zaire (Congo) deep-sea fan (ZaiAngo Project). *Marine Geology*, *209*(1-4), 223–244. https://doi.org/10.1016/j.margeo.2004.06.007

Athy, L. F. (1930). Density, porosity, and compaction of sedimentary rocks. *AAPG Bulletin*, *14*(1), 194–200. https://doi.org/10.1306/3D93289E-16B1-11D7-8645000102C1865D

Babault, J., Teixell, A., Arboleya, M. L., & Charroud, M. (2008). A late Cenozoic age for long-wavelength surface uplift of the Atlas Mountains of Morocco. *Terra Nova*, *20*(2), 102–107. https://doi.org/10.1111/j.1365-3121.2008.00794.x

Berggren, W. A., Kent, D. V., Swisher, C. C., & Aubry, M.-P. (1995). A revised Cenozoic geochronology and chronostratigraphy, Geochronology, Time Scales, and Global Stratigraphic Correlation. (54).

Blow, W. H. (1969). Late middle Eocene to Recent planktonic foraminiferal biostratigraphy. In: Proceedings of the First International Conference on Planktonic Microfossils. In *Proceedings of the first international conference on planktonic microfossils, geneva 1967* (pp. 199–422).

Bolli, H. M. (1957). Planktonic foraminifera from the Oligocene-Miocene Cipero and Lengua formation, Trinidad. *Bulletin of the United States National Museum*, *215*, 97–124.

Bolli, H. M. (1957). The genera Globigerina and Globorotaria in Paleocene-Lower Eocene Lizard Spring Formation of Trinidad, BWI. *Bulletin of the United States National Museum*, *215*, 61–81.

Bolli, HM, Saunders, JB, & Perch-Nielsen, K (1989). *Plankton stratigraphy, Planktic foraminifera, calcareous nannofossils and calpionellids* (Vol. 1): Cambridge Earth Science Series.

Bralower, T. J., Monechi, S., & Thierstein, H. R. (1989). Calcareous nannofossil zonation of the Jurassic-Cretaceous boundary interval and correlation with the geomagnetic polarity timescale. *Marine Micropaleontology*, *14*(1-3), 153–235. https://doi.org/10.1016/0377-8398(89)90035-2

Brown, P. R, Rutledge, D. C., Crux, J. A., & Gallagher, L. T. (1998). Early Cretaceous. In British Mi & P. R. Brown (Eds.), *Calcareous nannofossil biostratigraphy* (pp. 86–131). London: Chapman & Hall.

Brownfield, M. E., & Charpentier, R. R. (2003). Assessment of the undiscovered oil and gas of the Senegal Province, Mauritania, Senegal, The Gambia, and Guinea-Bissau, Northwest Africa. *U.S. Geological Survey Bulletin*, *2207-A*, 1–29.

Burke, K. (1996). The African plate. *South African Journal of Geology*, *99*(4), 341–409.

Burke, K., & Gunnell, Y. (2008). The African erosion surface: A continental-scale synthesis of geomorphology, tectonics, and environmental change over the past 180 million years. In *Memoir 201: The african erosion surface: A continental-scale synthesis of geomorphology, tectonics, and environmental change over the past 180 million years*. https://doi.org/10.1130/2008.1201

Burnett, J. A. (1998). Upper Cretaceous. In Mi British & P. R. Brown (Eds.), *Calcareous nannofossil biostratigraphy* (pp. 132–199). London: Chapman & Hall.

Chardon, D., Grimaud, J. L., Rouby, D., Beauvais, A., & Frederic, C. (2016). Stabilization of large drainage basins over geological time scales: Cenozoic West Africa, hot spot swell growth, and the Niger River. *Geochemistry, Geophysics, Geosystems*, *17*, 1164–1181. https://doi.org/10.1002/2015GC006169

Christensen, N. I. (1982). Seismic velocities. In R.S. Carmichael (Ed.), *handbook of physical properties of rocks* (pp. 57–74). Boca Raton, Fla: CRC Press.

Clift, P. D., & Sun, Z. (2006). The sedimentary and tectonic evolution of the Yinggehai-Song Hong basin and the southern Hainan margin, South China Sea: Implications for Tibetan uplift and monsoon intensification. *Journal of Geophysical Research*, *111*, B06405. https://doi.org/10.1029/2005JB004048

Croissant, T., & Braun, J. (2014). Constraining the stream power law: A novel approach combining a landscape evolution model and an inversion method. *Earth Surface Dynamics*, *2*(1), 155–166. https://doi.org/10.5194/esurf-2-155-2014

Crosby, A. G., Fishwick, S., & White, N. (2010). Structure and evolution of the intracratonic Congo Basin. *Geochemistry, Geophysics, Geosystems*, *11*, Q06010. https://doi.org/10.1029/2009GC003014

Crosby, B. T., & Whipple, K. X. (2006). Knickpoint initiation and distribution within fluvial networks: 236 waterfalls in the Waipaoa River, North Island, New Zealand. *Geomorphology*, *82*, 16–38. https://doi.org/10.1016/j.geomorph.2005.08.023

Czarnota, K., Roberts, G. G., White, N. J., & Fishwick, S. (2014). Spatial and temporal patterns of Australian dynamic topography from river profile modeling. *Journal of Geophysical Research: Solid Earth*, *119*, 1384–1424. https://doi.org/10.1002/2013JB010436

Daly, M. C., Chorowicz, J., & Fairhead, J. D. (1989). Rift basin evolution in Africa: The influence of reactivated steep basement shear zones. *Geological Society, London, Special Publications*, *44*, 309–334. https://doi.org/10.1144/GSL.SP.1989.044.01.17

Davison, I. (2005). Central Atlantic margin basins of North West Africa: Geology and hydrocarbon potential (Morocco to Guinea). *Journal of African Earth Sciences*, *43*, 254–274. https://doi.org/10.1016/j.jafrearsci.2005.07.018

Dingle, R. V. (1983). Continental margin subsidence: A comparison between east and west coasts of Africa. *Dynamics of passive margins*, *13*, 59–71.

DuToit, S., Kidston, A., & Slind, O. (1997). *The hydrocarbon potential of the east Africa continental margin*. Toronto, Canada: Alconsult International Ltd.

Elmejdoub, N., & Jedoui, Y. (2009). Pleistocene raised marine deposits of the Cap Bon peninsula (N-E Tunisia): Records of sea-level highstands, climatic changes and coastal uplift. *Geomorphology*, *112*(3-4), 179–189. https://doi.org/10.1016/j.geomorph.2009.06.001

Emery, K. O., & Uchupi, E. (1984). *The geology of the Atlantic Ocean*. New York: Springer-Verlag.

Erlanger, E. D., Granger, D. E., & Gibbon, R. J. (2012). Rock uplift rates in South Africa from isochron burial dating of fluvial and marine terraces. *Geology*, *40*(11), 1019–1022. https://doi.org/10.1130/G33172.1

Förste, C., Bruinsma, Sean. L., Abrikosov, O., Lemoine, J. M., Marty, J. C., Flechtner, F., et al. (2014). EIGEN-6C4 The latest combined global gravity field model including GOCE data up to degree and order 2190 of GFZ Potsdam and GRGS Toulouse. https://doi.org/10.5880/icgem.2015.1

Fairhead, J. D. (1988). Late Mesozoic rifting in Africa. *Developments in Geotectonics*, *22*, 821–831. https://doi.org/10.1016/B978-0-444-42903-2.50038-5

Fairhead, J. D. (1988). *Mesozoic plate tectonic reconstructions of the central South Atlantic Ocean: The role of the West and Central African rift system*. Amsterdam: Eisevier Science Publishers B.V.https://doi.org/10.1016/0040-1951(88)90265-X

Farr, T., Rosen, P., Caro, E., Crippen, R., Duren, R., Hensley, S., et al. (2007). The Shuttle Radar Topography Mission. *Reviews of Geophysics*, *45*, RG2004. https://doi.org/10.1029/2005RG000183.1

Goren, L., Fox, M., & Willett, S. D. (2014). Tectonics from fluvial topography using formal linear inversion: Theory and applications to the Inyo Mountains, California. *Journal of Geophysical Research: Earth Surface*, *119*, 1651–1681. https://doi.org/10.1002/2014JF003079

Grimaud, J. L., Rouby, D., Chardon, D., & Beauvais, A. (2018). Cenozoic sediment budget of West Africa and the Niger delta. *Basin Research*, *30*(2), 169–186. https://doi.org/10.1111/bre.12248

Guiraud, M., Buta-Neto, A., & Quesne, D. (2010). Segmentation and differential post-rift uplift at the Angola margin as recorded by the transform-rifted Benguela and oblique-to-orthogonal-rifted Kwanza basins. *Marine and Petroleum Geology*, *27*(5), 1040–1068. https://doi.org/10.1016/j.marpetgeo.2010.01.017

Gurnis, M., Mitrovica, J. X., Ritsema, J., & Van Heijst, H. J. (2000). Constraining mantle density structure using geological evidence of surface uplift rates: The case of the African Superplume. *Geochemistry, Geophysics, Geosystems*, *1*, 1020. https://doi.org/10.1029/1999GC000035

Hack, J. (1957). Studies of longitudinal stream profiles in Virginia and Maryland. USGS Professional Paper 249.

Hafid, M., Salem, A. A., & Bally, A. W. (2000). The western termination of the Jebilet High Atlas system (offshore Essaouira Basin, Morocco). *Marine and Petroleum Geology*, *17*(3), 431–443. https://doi.org/10.1016/S0264-8172(98)00082-8

Hall, J., Krasheninnikov, V., Hirsch, F., Benjamini, C., Flexer, A., & Hall, J. (2005). Geological framework of the Levant. *Volume II: The Levantine*, *2*, 836. https://doi.org/10.1016/j.gloenvcha.2011.08.005

Hancock, G. R., Martinez, C., Evans, K. G., & Moliere, D. R. (2006). A comparison of SRTM and high-resolution digital elevation models and their use in catchment geomorphology and hydrology: Australian examples. *Earth Surface Processes and Landforms*, *31*, 1394–1412. https://doi.org/10.1002/esp.1335

Hobley, D. E. J., Adams, J. M., Nudurupati, S. S., Hutton, E. W. H., Gasparini, N. M., Istanbulluoglu, E., & Tucker, G. E. (2017). Creative computing with Landlab: An open source toolkit for building, coupling, and exploring two-dimensional numerical models of Earth-surface dynamics. *Earth Surface Dynamics*, *5*, 21–46. https://doi.org/10.5194/esurf-5-21-2017

Hoggard, M. J., Winterbourne, J., Czarnota, K., & White, N. (2017). Oceanic residual depth measurements, the plate cooling model, and global dynamic topography. *Journal of Geophysical Research: Solid Earth*, *122*, 2328–2372. https://doi.org/10.1002/2016JB013457

Holmes, A. (1944). *Principles of Physical Geology*. London and Edinburgh, UK: Thomas Nelson and Sons.

Howard, A. (1971). Problems in interpretation of simulation models of geologic processes. In P. M. Morisawa (Ed.), *Quantitative Geomorphology: Some Aspects and Applications* (pp. 61–82). Binghamton, NY: Geomorphology.

Howard, A. D. (1987). Modelling fluvial systems: Rock-, gravel-, and sand-bed channels. In *River Channels: Environment and Process*. Oxford, UK.

Howard, A. D. (1988). Equilibrium models in geomorphology. In M. Anderson (Ed.), *Modelling geomorphological systems* (pp. 49–70). New York, USA: John Wiley.

Howard, A. D., Dietrich, W. E., & Seidl, M. A. (1994). Modeling fluvial erosion on regional to continental scale. *Journal of Geophysical Research*, *99*, 13,971–13,986.

Howard, A. D., & Hemberger, A. T. (1991). Multivariate characterization of meandering. *Geomorphology*, *4*(3-4), 161–186. https://doi.org/10.1016/0169-555X(91)90002-R

Howard, A. D., & Kerby, G. G. (1983). Channel changes in badlands. *Geological Society of America Bulletin*, *94*(6), 739–752. https://doi.org/10.1130/0016-7606

Immenhauser, A. (2009). Estimating palaeo-water depth from the physical rock record. *Earth-Science Reviews*, *96*(1-2), 107–139. https://doi.org/10.1016/j.earscirev.2009.06.003

Ismail, A. A., Boukhary, M., & Naby, AhmedIAbdel (2010). Subsurface stratigraphy & micropaleontology of the Neogene rocks, Nile Delta, Egypt. *Geologia Croatica*, *63*(1), 1–26. https://doi.org/104154/gc.2010.01

Janssen, M. E., Stephenson, R. A., & Cloetingh, S. (1995). Temporal and spatial correlations between changes in plate motions and the evolution of rifted basins in Africa. *Geological Society of America Bulletin*, *107*(11), 1317–1332. https://doi.org/10.1130/0016-7606

Jardiné, S., & Magloire, L. (1965). Palynologie et stratigraphie du Crétacé des basins du Sénégal et de Côte d'Ivoire, Mémoire du Bureau Recherche Géologiques Minières.

Jones, S. M., Lovell, B., & Crosby, A. G. (2012). Comparison of modern and geological observations of dynamic support from mantle convection. *Journal of the Geological Society*, *169*(6), 745–758. https://doi.org/10.1144/jgs2011-118

Kennett, J. P., & Srinivasan, M. S. (1983). *Neogene planktonic foraminifera*. Stroudsburg, Pennsylvania: Hutchinson Ross Publ. Go.

Lague, D. (2014). The stream power river incision model: Evidence, theory and beyond. *Earth Surface Processes and Landforms*, *39*(1), 38–61. https://doi.org/10.1002/esp.3462

Leckie, R. M., Farnham, C., & Schmidt, M. G. (1993). Oligocene planktonic foraminifer biostratigraphy of Hole 803D (Ontong Java Plateau) and Hole 628A (Little Bahama Bank), and comparison with the southern high latitudes. *Proceedings of the Ocean Drilling Program, 130 Scientific Results*, *130*, 113–136. https://doi.org/10.2973/odp.proc.sr.130.012.1993

Lodhia, B. H., Roberts, G. G., Fraser, A. J., Fishwick, S., Goes, S., & Jarvis, J. (2018). Continental margin subsidence from shallow mantle convection: Example from West Africa. *Earth and Planetary Science Letters*, *481*, 350–361. https://doi.org/10.1016/j.epsl.2017.10.024

Loget, N., Davy, P., & Van Den Driessche, J. (2006). Mesoscale fluvial erosion parameters deduced from modeling the Mediterranean sea level drop during the Messinian (late Miocene). *Journal of Geophysical Research*, *111*, F03005. https://doi.org/10.1029/2005JF000387

McKenzie, D., & Fairhead, D. (1997). Estimates of the effective elastic thickness of the continental lithosphere from Bouguer and free air gravity anomalies. *Journal of Geophysical Research*, *102*(B12), 27,523–27,552. https://doi.org/10.1029/97JB02481

Meghraoui, M., Outtani, F., Choukri, A., & De Lamotte, D. F. (1998). Coastal tectonics across the South Atlas thrust front and the Agadir active zone, Morocco. *Geological Society London Special Publications*, *146*(1), 239–253. https://doi.org/10.1144/GSL.SP.1999.146.01.14

Milliman, J. D., & Farnsworth, K. L. (2013). *River discharge to the coastal ocean: A global synthesis*. Cambridge, UK: Cambridge University Press.

Milliman, J., & Syvitski, J. (1992). Geomorphic/tectonic control of sediment discharge to the ocean: The importance of small mountainous rivers. *The Journal of Geology*, *100*(5), 525–544.

Monechi, S., Reale, V., Bernaola, G., & Balestra, B. (2013). The Danian/Selandian boundary at Site 1262 (South Atlantic) and in the Tethyan region: Biomagnetostratigraphy, evolutionary trends in fasciculiths and environmental effects of the Latest Danian Event. *Marine Micropaleontology*, *98*, 28–40. https://doi.org/10.1016/j.marmicro.2012.11.002

Moucha, R., & Forte, A. M. (2011). Changes in African topography driven by mantle convection. *Nature Geoscience*, *4*(10), 707–712. https://doi.org/10.1038/ngeo1235

Mudd, S. M., Attal, M., Milodowski, D. T., Grieve, S. W., & Valters, D. A. (2014). A statistical framework to quantify spatial variation in channel gradients using the integral method of channel profile analysis. *Journal of Geophysical Research: Earth Surface*, *119*, 138–152. https://doi.org/10.1002/2013JF002981

Nyagah, K. (1995). Stratigraphy, depositional history and environments of deposition of Cretaceous through Tertiary strata in the Lamu Basin, southeast Kenya and implications for reservoirs for hydrocarbon exploration. *Sedimentary Geology*, *96*(1-2), 43–71. https://doi.org/10.1016/0037-0738(94)00126-F

Nyblade, A. A., & Robinson, S. W. (1994). The African Superswell. *Geophysical Research Letters*, *21*(9), 765–768. https://doi.org/10.1029/94GL00631

Olsson, R. K., Berggren, W. A., Hemleben, C. I., & Huber, B. T. (1999). Atlas of Paleocene planktonic foraminifera.

Olsson, R. K., Pearson, P. N., & Huber, B. T. (2006). Taxonomy, biostratigraphy, and phylogeny of Eocene Catapsydrax, Globorotaloides, Guembelitrioides, Paragloborotalia, Parasubbotina, and Pseudoglobigerinella n. gen. In F. Cushman et al. (Eds.), *Atlas of eocene planktonic foraminifera* (pp. 67–110). Lawrence, Kansas: Allen Press.

Partridge, T. C. (1998). Of diamonds, dinosaura and diastrophism: 150 million years of landscape evolution in southern Africa. *South African Journal of Geology*, *101*(3), 167–184.

Partridge, T., & Maud, R. (1987). Geomorphic evolution of southern Africa since the Mesozoic. *South African Journal of Geology*, *90*(2), 179–208.

Partridge, T. C., & Maud, R. R. (2000). Macro-scale geomorphic evolution of southern Africa, *The Cenozoic of Southern Africa* (Vol. 40, pp. 3–18). New York: Oxford University Press.

Paul, J. D., Roberts, G. G., & White, N. (2014). The African landscape through space and time. *Tectonics*, *33*, 898–935. https://doi.org/10.1002/2013TC003479.

Perch-Nielsen, K. (1977). Albian to Pleistocene calcareous nannofossils from the Western South Atlantic, DSDP Leg 39. *Initial Reports of the Deep Sea Drilling Project*, *39*, 699–823. https://doi.org/10.2973/dsdp.proc.39.131.1977

Perch-Nielsen, K., Sadek, A., Barakat, M. G., & Teleb, F. (1978). Late Cretaceous and Early Tertiary calcareous nannofossil and planktonic foraminifera zones from Egypt. *Actes du VIe Colloque Africain de Micropaléontologie, Tunis: Annales des Mines et de la Géologie*, *28*(2), 337–403.

Plummer, H. J. (1931). Some Cretaceous foraminifera in Texas. *University of Texas bull*, *3101*, 109–203.

Pritchard, D., Roberts, G. G., White, N. J., & Richardson, C. N. (2009). Uplift histories from river profiles. *Geophysical Research Letters*, *36*, L24301. https://doi.org/10.1029/2009GL040928

Reijers, T. J. A. (2011). Stratigraphy and sedimentology of the Niger delta. *Geologos*, *17*(3), 133–162. https://doi.org/10.2478/v10118-011-0008-3

Roberts, D. L., & Brink, J. S. (2002). Dating and correlation of neogenecoastal deposits in the Western Cape (South Africa): Implications for neotectonism. *South African Journal of Geology*, *105*, 337–352.

Roberts, G. G., Paul, J. D., White, N., & Winterbourne, J. (2012a). Temporal and spatial evolution of dynamic support from river profiles: A framework for Madagascar. *Geochemistry, Geophysics, Geosystems*, *13*, Q04004. https://doi.org/10.1029/2012GC004040

Roberts, G. G., & White, N. (2010). Estimating uplift rate histories from river profiles using African examples. *Journal of Geophysical Research*, *115*, B02406. https://doi.org/10.1029/2009JB006692

Roberts, G., White, N., & Lodhia, B. (2019). The generation and scaling of longitudinal river profiles. *Journal of Geophysical Research: Earth Surface*, *124*, 137–153. https://doi.org/10.1029/2018JF004796

Roberts, G. G., White, N. J., Martin-Brandis, G. L., & Crosby, A. G. (2012b). An uplift history of the Colorado Plateau and its surroundings from inverse modeling of longitudinal river profiles. *Tectonics*, *31*, TC4022. https://doi.org/10.1029/2012TC003107

Romein, A. J. T. (1979). Lineages in early Paleogene calcareous nannoplankton. *Utrecht Micropaleontological Bulletins*, *22*, 1–230.

Rosenbloom, N. A., & Anderson, R. S. (1994). Hillslope and channel evolution in a marine terraced landscape, Santa Cruz, California. *Journal of Geophysical Research*, *99*(B7), 14,013–14,029. https://doi.org/10.1029/94JB00048

Rouby, D., Bonnet, S., Guillocheau, F., Gallagher, K., Robin, C., Biancotto, F., et al. (2009). Sediment supply to the Orange sedimentary system over the last 150 My: An evaluation from sedimentation/denudation balance. *Marine and Petroleum Geology*, *26*(6), 782–794. https://doi.org/10.1016/j.marpetgeo.2008.08.004.

Royden, L., & Perron, J. T. (2013). Solutions of the stream power equation and application to the evolution of river longitudinal profiles. *Journal of Geophysical Research: Earth Surface*, *118*, 497–518. https://doi.org/10.1002/jgrf.20031.

Rudge, J. F., Roberts, G. G., White, N. J., & Richardson, C. N. (2015). Uplift histories of Africa and Australia from linear inverse modeling of drainage inventories. *Journal of Geophysical Research: Earth Surface*, *120*, 894–914. https://doi.org/10.1002/2014JF003297

Rust, D. J., & Summerfield, M. A. (1990). Isopach and borehole data as indicators of rifted margin evolution in southwestern Africa. *Marine and Petroleum Geology*, *7*(3), 277–287. https://doi.org/10.1016/0264-8172(90)90005-2

Sahagian, D. (1988). Epeirogenic motions of Africa as inferred from Cretaceous shoreline deposits. *Tectonics*, *7*(1), 125–138. https://doi.org/10.1029/TC007i001p00125

Said, A., Moder, C., Clark, S., & Ghorbal, B. (2015). Cretaceous-Cenozoic sedimentary budgets of the Southern Mozambique Basin: Implications for uplift history of the South African Plateau. *Journal of African Earth Sciences*, *109*, 1–10. https://doi.org/10.1016/j.jafrearsci.2015.05.007

Salles, T., Ding, X., & Brocard, G. (2018). pyBadlands: A framework to simulate sediment transport, landscape dynamics and basin stratigraphic evolution through space and time. *PLoS ONE*, *13*(4), e0195557.

Salman, G., & Abdula, I. (1995). Development of the Mozambique and Ruvuma sedimentary basins, offshore Mozambique. *Sedimentary Geology*, *96*(1-2), 7–41. https://doi.org/10.1016/0037-0738(95)00125-R

Séranne, M., & Nzé Abeigne, C. R. (1999). Oligocene to Holocene sediment drifts and bottom currents on the slope of Gabon continental margin (west Africa) consequences for sedimentation and southeast Atlantic upwelling. *Sedimentary Geology*, *128*(3-4), 179–199. https://doi.org/10.1016/S0037-0738(99)00069-X

Sestini, G. (1989). Nile delta: A review of depositional environments and geological history. *Geological Society, London, Special Publications*, *41*(1), 99–127. https://doi.org/10.1144/GSL.SP.1989.041.01.09

Sigal, J. (1948). Notes sur les genres de foraminiferes Rotalipora Brotzen, 1942 et Thalmanninella (Famille des Globorotaliidae). *Revue de l'Institut Francais du Petrole et Annales des Combustible Liquides*, *3*(4), 95–103.

Sklar, L., & Dietrich, W. E. (1998). River longitudinal profiles and bedrock incision models: Stream power and the influence of sediment supply. *Geophysical Monograph Series*, *107*, 237–260. https://doi.org/10.1029/GM107p0237

Sklar, L. S., & Dietrich, W. E. (2001). Sediment and rock strength control on river incision into bedrock. *Geology*, *29*(12), 1087–1090. https://doi.org/10.1130/0091-7613

Smith, W. H. F., & Wessel, P. (1990). Gridding with continuous curvature splines in tension. *Geophysics*, *55*(3), 293–305.

Somme, T. O., Piper, D. J. W., Deptuck, M. E., & Helland-Hansen, W. (2011). Linking onshore-offshore sediment dispersal in the Golo source-to-sink system (Corsica,France) during the Late Quaternary. *Journal of Sedimentary Research*, *81*(2), 118–137. https://doi.org/10.2110/jsr.2011.11

Stephenson, S., Roberts, G., Hoggard, M., & Whittaker, A. (2014). From longitudinal river profiles. *Geochemistry, Geophysics, Geosystems*, *15*, 4734–4758. https://doi.org/10.1002/2014GC005425.Received

Tomkin, J. H., Brandon, M. T., Pazzaglia, F. J., Barbour, J. R., & Willett, S. D. (2003). Quantitative testing of bedrock incision models for the Clearwater River, NW Washington State. *Journal of Geophysical Research*, *108*(B6), 2308. https://doi.org/10.1029/2001JB000862

Van der Beek, P., & Bishop, P. (2003). Cenozoic river profile development in the Upper Lachlan catchment (SE Australia) as a test of quantitative fluvial incision models. *Journal of Geophysical Research*, *108*(B6), 2309. https://doi.org/10.1029/2002JB002125

Varol, O. (1989). Palaeocene calcareous nannofossil biostratigraphy, *Nannofossils and their applications* (pp. 267–310). Chichester: Ellis Horwood Ltd.

Vear, A. (2005). Deep-water plays of the Mauritanian continental margin. *Petroleum Geology*, *6*(1), 1217–1232.

Villeneuve, M. (2005). Paleozoic basins in West Africa and the Mauritanide thrust belt. *Journal of African Earth Sciences*, *43*(1-3), 166–195. https://doi.org/10.1016/j.jafrearsci.2005.07.012

Wade, B. S., Pearson, P. N., Berggren, W. A., & Pälike, H. (2011). Review and revision of Cenozoic tropical planktonic foraminiferal biostratigraphy and calibration to the geomagnetic polarity and astronomical time scale. *Earth-Science Reviews*, *104*(1-3), 111–142. https://doi.org/10.1016/j.earscirev.2010.09.003

Walford, H. L., White, N. J., & Sydow, J. C. (2005). Solid sediment load history of the Zambezi Delta. *Earth and Planetary Science Letters*, *238*(1-2), 49–63. https://doi.org/10.1016/j.epsl.2005.07.014.

Walker, K. R., Shanmugam, G., & Ruppel, S. C. (1983). A model for carbonate to terrigenous clastic sequences. *Geological Society of America Bulletin*, *94*(6), 700–712. https://doi.org/10.1130/0016-7606

Weissel, J. K., & Seidl, M. A. (1998). Inland propagation of erosional escarpments and river profile evolution across the southeast Australian passive continental margin. *Geophysical Monograph Series*, *107*, 189–206. https://doi.org/10.1029/GM107p0189

Whipple, K. X., & Tucker, G. E. (1999). Dynamics of the stream-power river incision model: Implications for height limits of mountain ranges, landscape response timescales, and research needs. *Journal of Geophysical Research*, *104*(B8), 17,661–17,674. https://doi.org/10.1029/1999JB900120

Whittaker, A. C., & Boulton, S. J. (2012). Tectonic and climatic controls on knickpoint retreat rates and landscape response times. *Journal of Geophysical Research*, *117*, F02024. https://doi.org/10.1029/2011JF002157

Whittaker, A. C., Cowie, P. A., Attal, M., Tucker, G. E., & Roberts, G. P. (2007). Bedrock channel adjustment to tectonic forcing: Implications for predicting river incision rates. *Geology*, *35*(2), 103–106. https://doi.org/10.1130/G23106A.1

Whittaker, J. M., Goncharov, A., Williams, S. E., Müller, R. Dietmar, & Leitchenkov, G. (2013). Global sediment thickness data set updated for the Australian-Antarctic Southern Ocean. *Geochemistry, Geophysics, Geosystems*, *14*, 3297–3305. https://doi.org/10.1002/ggge.20181

Wyllie, M. R. J., Gregory, A. R., & Gardner, L. W. (1956). Elastic wave velocities in heterogeneous and porous media. *Geophysics*, *21*(1), 41–70. https://doi.org/10.1190/1.1438217

Young, J. R., Bown, P. R., & Lees, J. A. (2018). Guembelitria sp. http://www.mikrotax.org/pforams/index.php?taxon=Guembelitriasp.&module=pf_cenozoic